

# Spatiotemporal Implicit Neural Representation as a Generalized Traffic Data Learner

Tong Nie<sup>a,b</sup>, Guoyang Qin<sup>a</sup>, Wei Ma<sup>b,\*</sup>, Jian Sun<sup>a,\*</sup>

<sup>a</sup>Department of Traffic Engineering, Tongji University, Shanghai, 201804, China

<sup>b</sup>Department of Civil and Environmental Engineering, The Hong Kong Polytechnic University, Hong Kong SAR, China

---

## Abstract

Spatiotemporal Traffic Data (STTD) measures the complex dynamical behaviors of the multiscale transportation system. Existing methods aim to reconstruct STTD using low-dimensional models. However, they are limited to data-specific dimensions or source-dependent patterns, restricting them from unifying representations. Here, we present a novel paradigm to address the STTD learning problem by parameterizing STTD as an implicit neural representation. To discern the underlying dynamics in low-dimensional regimes, coordinate-based neural networks that can encode high-frequency structures are employed to directly map coordinates to traffic variables. To unravel the entangled spatial-temporal interactions, the variability is decomposed into separate processes. We further enable modeling in irregular spaces such as sensor graphs using spectral embedding. Through continuous representations, our approach enables the modeling of a variety of STTD with a unified input, thereby serving as a generalized learner of the underlying traffic dynamics. It is also shown that it can learn implicit low-rank priors and smoothness regularization from the data, making it versatile for learning different dominating data patterns. We validate its effectiveness through extensive experiments in real-world scenarios, showcasing applications from corridor to network scales. Empirical results not only indicate that our model has significant superiority over conventional low-rank models, but also highlight that the versatility of the approach extends to different data domains, output resolutions, and network topologies. Comprehensive model analyses provide further insight into the inductive bias of STTD. We anticipate that this pioneering modeling perspective could lay the foundation for universal representation of STTD in various real-world tasks.

*Keywords:* Implicit neural representations, Traffic data learning, Spatiotemporal traffic data, Traffic dynamics, Multilayer perceptron

---

## 1. Introduction

The heterogeneous elements involved in a vehicular traffic system, such as travel demand, human behaviors, infrastructure supply, weather conditions, and social economics, lead to a complex, high-dimensional, and large-scale dynamical system (Avila and Mezić, 2020). To better understand this system, spatiotemporal traffic data (STTD) is a quantity that is often collected to describe its evolution in space and time (Yuan and Li, 2021). This data includes various sources such as vehicle trajectories, sensor-based time series, and dynamic mobility flow, which is measured either by Eulerian measurements at fixed locations or Lagrangian measurements from mobile sensors. Traffic participants are constantly immersed in STTD, perceiving it through the daily travels of moving agents, recording it through different types of traffic detectors, and finally analyzing and utilizing it.

In practical traffic engineering, STTD is one of the main ingredients required to provide vital information for the timely and effective deployment of large-scale traffic control strategies (Tsitsokas et al., 2023; Hu and Ma, 2024), data-driven traffic demand management (Nallaperuma et al., 2019), and elaborate traffic optimization routines (Wang et al., 2024) in modern intelligent transportation systems (Zhang et al., 2011). Meanwhile, the ever-increasing amount of STTD in transportation systems has left traffic agencies in need of a generalized method to analyze the continuously collected data in various types. However, one can face the challenge of fully understanding the mystery of STTD, which can be caused by multiple interwoven factors. For example, traffic congestion dynamics involves entangled relationships between spatial and temporal domains (Bellocchi and Geroliminis, 2020; Saberi et al., 2020; Duan et al., 2023), and the high dimensionality of STTD further intensifies the challenges in data processing (Asif et al., 2013). These difficulties undermine its direct utility in reality.

STTD modeling has gained greater attention in the field of traffic data science and engineering in recent years. To dissect the spatiotemporal complexity, the primary aim of STTD learning is to develop data-centric learners

---

\*Corresponding authors.

Email addresses: wei.w.ma@polyu.edu.hk (Wei Ma), sunjian@tongji.edu.cn (Jian Sun)

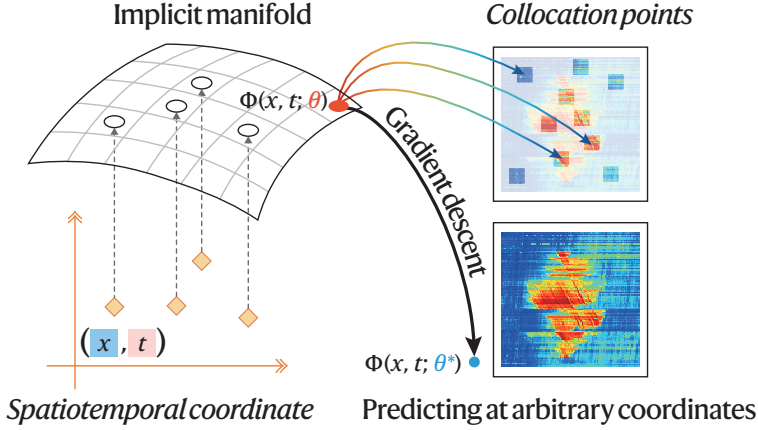
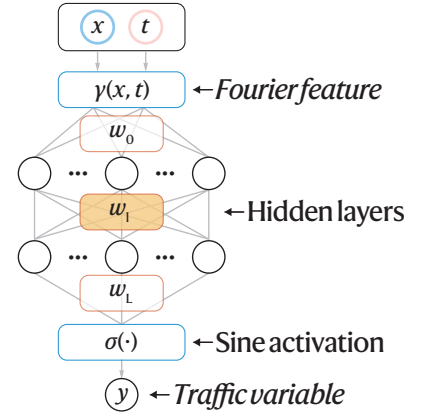
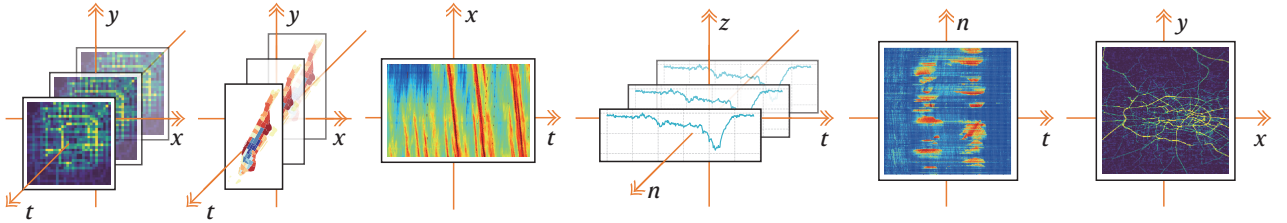
**a. Representing traffic data as continuous functions****b. Coordinate-based MLPs****c. Multiscale spatiotemporal traffic data**

Figure 1: **Representing spatiotemporal traffic data as an implicit neural function.** (a) Traffic data at arbitrary spatial-temporal coordinates can be represented as a continuous function in an implicit space. (b) Coordinate-based MLPs map input coordinates to traffic state of interest. (c) With the resolution-independent property, our model can learn a variety of spatiotemporal traffic data from different sources.

that can accurately *learn predictive functions from observations and predict complex dynamics of STTD*. In this sense, the system that generates STTD can be characterized as a nonlinear dynamical system that exhibits abundant multiscale and interactive phenomena. Despite its complexity, recent advances in STTD have found that the dynamics of the system evolve with some dominating patterns and can be captured by some low-dimensional structures (Thibeault et al., 2024; Wu et al., 2024). Notably, low-rankness is a widely studied structure. The low-rank learner uses the algebraic structures of STTD and organizes it into a matrix or a tensor format (Asif et al., 2016). Models based on it assist in reconstructing sparse data (Tan et al., 2013; Wang et al., 2018; Chen et al., 2019a; Nie et al., 2022; Lyu et al., 2024), detecting anomalies (Wang et al., 2021; Sofuoglu and Aviyente, 2022), revealing patterns (Avila and Mezić, 2020; Wang and Sun, 2023), forecasting future variables (Yang et al., 2021), and predicting unknown states (Zhang et al., 2020; Nie et al., 2023b; Wang et al., 2023; Xing et al., 2023).

While great progress has been made by using low-rank models as learners of STTD, these methods have focused either on patterns that are applicable to specific data structures and dimensions or have demonstrated state-of-the-art results with source-dependent priors. This limits the potential for a unified representation and emphasizes the need for a generally applicable method to link various types of STTD learning. To address these limitations, we first carefully survey existing low-rank models and have identified the primary shortcomings that hinder their versatility. (1) *Absence of high-frequency components*: The rationale for low-rank models is to completely remove high-frequency components and treat them as noise. However, high-frequency components can provide informative details for the accurate reconstruction of spatial-temporal fields (Luo et al., 2024). Omitting this section of the signals will lead to a loss of information such as nonrecurrent events and phase transitions. (2) *Resolution dependency*: Due to the matrix or tensor organization, these models are restricted to regular sampling intervals or discrete mesh grids. They often require a grid-based input with fixed spatiotemporal dimensions, restricting them from accommodating varying spatial resolutions or temporal lengths. Such a restriction makes them infeasible to work beyond the current discretization, which violates the continuous nature of STTD. More importantly, STTD is sometimes sensitive to the choice of discretization. For example, the definition of a space-time cell has an obvious impact on the reproduction of congestion wave (He et al., 2017). In addition, they are also memory intensive because the discrete representation requires the entire input of numerous grids. (3) *Explicit regularization*: To ensure favorable performance, some structural priors are usually explicitly imposed on standard low-rank models. For instance, a predefined small rank or a surrogate norm function is necessary to facilitate the optimization process (Goulart et al., 2017; Chen et al., 2020). Such a rank or norm selection procedure can be tricky, and the low-rank pattern modeling, fixed on one data source, may not generalize to different data sources. For instance, low-rankness identified in one data type, such as vehicle trajectories, may not be applicable

to differently structured data, such as OD demand. Moreover, some prior regularization terms are also needed to regulate the local consistency of STTD (Yu et al., 2016; Chen et al., 2022; Nie et al., 2023b). These hand-crafted a priori are eventually processed into heuristic penalty functions and a choice of several hyperparameters, which are scenario-based and less adaptable to different problems.

To unravel these difficulties, we attempt to learn the data-generating dynamics of STTD directly. Fortunately, deep learning approaches exist for a promising facet of this problem. Recent studies have empirically demonstrated the surprising ability of deep neural networks to learn predictive representations of dynamical systems, such as physics-informed neural networks for traffic speed and density field estimation (Huang and Agarwal, 2020; Shi et al., 2021; Zhang et al., 2024; Zheng et al., 2024). However, it seems impossible to derive authentic governing equations or explicit regularities of these complex traffic dynamics in all scenarios due to unpredictable factors in real-world conditions. This prompts us to develop data-driven *implicit* techniques. Recently, there has been a rise in the prominence of implicitly defined, continuous, and expressive data representation models parameterized by deep neural networks. This novel paradigm uses neural networks to discern patterns from continuous input. It has proven to be powerful in representing images, videos, and point cloud data, offering numerous advantages over traditional representations (Sitzmann et al., 2020; Tancik et al., 2020; Chen et al., 2021c). The implicit neural presentations (INRs) function in a continuous function space and take domain coordinates as input, predicting the corresponding quantity at the queried coordinates. INRs directly model the mapping from low-dimensional regimes, such as coordinates and derivatives, to high-frequency structures, which is necessary to represent processes defined implicitly by some governing dynamics. This differentiates them from low-rank models that depend on explicit dominating patterns, enhancing their expressivity in learning complex data details, and enabling them to fit processes that generate target data with functional representation. Consequently, the continuous representations eliminate the need for fixed data dimensions and can adjust to STTD of any scale or resolution, allowing us to model various STTD with a unified input. In this work, we exploit the advances of INRs and tailor them to incorporate the characteristics of STTD, resulting in a novel method that serves as a general traffic data learner (see Fig. 1a).

Specifically, we parameterize the implicit mapping from input domain to traffic states using coordinate-based multilayer perceptrons (MLPs) (see Fig. 1b). To learn complex details within the definition domain, we encode high-frequency components into the input of MLPs. To unravel the entangled relationships between spatial and temporal factors, we decompose the variability into separate processes through coordinate disentanglement. To model STTD exists in irregular space such as a sensor graph, we formulate a spectral embedding technique to learn non-Euclidean mappings. In addition to the versatility of the representation, we also theoretically show that it possesses several salient features that are crucial for STTD in practical applications. They include: (i) implicit low-rank regularization derived from the gradient descent over deep matrix factorization; (ii) inherent smoothness from the continuity of MLPs; and (iii) reduced computational complexity. As a result, the proposed method explicitly encodes high-frequency structures to learn complex details of STTD while at the same time implicitly learning low-rank and smooth priors from data to reconstruct the dominating modes. Through the lens of generalized representations, we can explore the possibility of developing a task-agnostic base learner that can predict the collective behaviors of STTD and address a wide variety of learning problems in reality (see Fig. 1c).

Our proof-of-concept has shown promising results through extensive evaluations using real-world datasets. The proposed learner is versatile, working across different scales - from corridor-level to network-level applications. It can also be generalized to various input dimensions, data domains, output resolutions, and network topologies. Comprehensive model analyses are also provided to fully examine its working mechanism. This study offers novel perspectives on STTD modeling and provides an extensive analysis of practical applications, contributing to state-of-the-art STTD learning methods. To our knowledge, this is the first time that INRs have been effectively applied to STTD learning and have demonstrated promising results in a variety of real-world tasks. We anticipate this could form the basis for developing foundational models for STTD. Our main contributions are summarized as follows:

1. A new paradigm for generalized STTD learning is presented that parameterizes traffic variables as an implicit mapping of domain coordinates;
2. A coordinate disentanglement strategy is proposed to dissect the complexity of learning on full domains and a graph spectral embedding technique is developed to model irregular data on topological spaces;
3. Salient analytical properties of our model that can serve as regularization for STTD are provided, including high-frequency encoding, implicit low-rankness, and inherent smoothness;
4. Our comprehensive experiments provide the first practice that demonstrates the effectiveness of INRs on extensive real-world STTD learning problems, covering data from micro to macro scales.

The remainder of this paper is organized as follows. Section 2 reviews the existing work on STTD according to different tasks. Section 3 introduces the STTD learning problem, elaborates on our method, and performs a theoretical analysis. Section 4 evaluates it on several real-world scenarios. Section 5 discusses the modular designs in detail. Section 6 concludes this work and provides future directions.

## 2. Related Works

Existing approaches for STTD span multiple research areas and are briefly discussed in this section to recapitulate the motivation of our paper. In particular, we detail low-rank methods for traffic data reconstruction as a representative. We also briefly review the recent advances of INRs in the machine learning community.

### 2.1. Spatiotemporal traffic data modeling

Since STTD can be generated on various scales of transportation systems, it has a wide spectrum of applications. Current studies usually combine data-driven models with STTD to achieve a particular modeling purpose. Representative tasks include: data reconstruction on road segment (Wang et al., 2018; Bae et al., 2018), graph-based sensor data imputation (Deng et al., 2021), deep learning-based imputation (Shi et al., 2021; Liang et al., 2022a,b; Nie et al., 2023a), prediction of unmeasured traffic on urban road segment (Zhang et al., 2020), highway speed extrapolation (kriging) (Wu et al., 2021; Nie et al., 2023b), highway traffic volume estimation (Nie et al., 2023c), transfer-based volume estimation (Zhang et al., 2022), anomaly detection (Qin et al., 2019; Wang et al., 2021), data denoising (Zheng et al., 2024), learning relational structures (Lei et al., 2022), dynamics modeling and analysis (Avila and Mezić, 2020; Lehmborg et al., 2021; Wang and Sun, 2023), forward and backward dynamics modeling (Thodi et al., 2024), real-time traffic forecasting (Yang et al., 2021), origin-destination flow forecasting (Zhang et al., 2021; Cheng et al., 2022), individual trajectory reconstruction (Chen et al., 2024), reconstruction of recurrent spatial-temporal traffic states at intersections (Wang et al., 2024), corridor speed field estimation (Wang et al., 2023), link travel time estimation (Li et al., 2023; Fu et al., 2023), estimating network-wide speed matrix (Liu et al., 2019; Yu et al., 2020), macroscopic network state estimation (Saeedmanesh et al., 2021), empirical analysis of large-scale multimodal network (Fu et al., 2020).

### 2.2. Low-rank models for spatiotemporal traffic data

Among the STTD modeling tasks, sensor-based traffic data imputation has attracted particular interest in recent years. In this problem, low-rank models are preferred for their simplicity and interpretability. The multivariate sensor time series is first organized into a spatiotemporal matrix or tensor, then low-rank models such as matrix factorization, nuclear norm minimization, tensor factorization, and tensor completion are adopted to fill in the missing data. A pioneering work (Tan et al., 2013) introduced a Tucker tensor model to model multidimensional traffic data. Asif et al. (2016) studied the effectiveness of different matrix- and tensor-based methods to estimate missing data in traffic systems. After these works, numerous studies have emerged to develop more advanced low-rank surrogates (Goulart et al., 2017; Zhang et al., 2019; Chen et al., 2019a,b, 2020, 2021a; Nie et al., 2022; Xing et al., 2023), propose new regularization schemes (Wang et al., 2018; Chen et al., 2022; Nie et al., 2023b), and integrate them with time series processing frameworks (Chen et al., 2021b; Wang et al., 2023; Lyu et al., 2024).

### 2.3. Implicit data and function representation

INRs are an emerging paradigm for representing data and functions in machine learning community, such as images, videos, 3D scenes, point cloud, and audio data (Sitzmann et al., 2020; Tancik et al., 2020; Mildenhall et al., 2021; Chen et al., 2021c; Dupont et al., 2021). In particular, Sitzmann et al. (2020) proposed a simple-yet-effective periodic activation to help INRs learn high-frequency features. Tancik et al. (2020) provided a in depth discussion on the role of Fourier features in deep neural networks using the theory of the neural tangent kernel. Mildenhall et al. (2021) developed a neural radiance fields model with positional encoding to synthesize novel views of complex scenes. A recent work (Luo et al., 2023) extended INRs to tensor structures and proposed a tensor functional representation for visual and point-cloud data. INRs have also been extended to model time series, termed time-index models (Fons et al., 2022; Naour et al., 2023; Woo et al., 2023). However, the application of INRs in spatiotemporal data, especially for traffic data, is still lacking.

## 3. ST-INR for Generalized Traffic Dynamics Learning

To begin with, this section first introduces the key concepts and notation used throughout the paper. Regarding the notation, we follow the terminology of (Kolda and Bader, 2009). Specifically, matrices are denoted by boldface capital letters e.g.,  $\mathbf{A} \in \mathbb{R}^{M \times N}$ , vectors are represented by boldface lowercase letters, e.g.,  $\mathbf{a} \in \mathbb{R}^M$  and scalars are lowercase letters, e.g.,  $a$ . Without ambiguity, functions are abbreviated as  $\Phi(\cdot)$ . Without special remarks, we use calligraphic letters to denote the vector space, e.g.,  $\mathcal{X} \subseteq \mathbb{R}$ . In particular, loss function is signified as  $\mathcal{L}(\cdot)$ . Next, we will elaborate the proposed spatiotemporal implicit neural representation (ST-INR) model. We will begin by introducing the generalized modeling framework from a broad perspective. Then we detail each modular design to account for the characterization of STTD. Finally, we provide theoretical discussions to indicate some important properties that are crucial for real-world applications. The overall architecture of the proposed ST-INR is shown in Fig. 2 (three-dimensional data is used as an example).



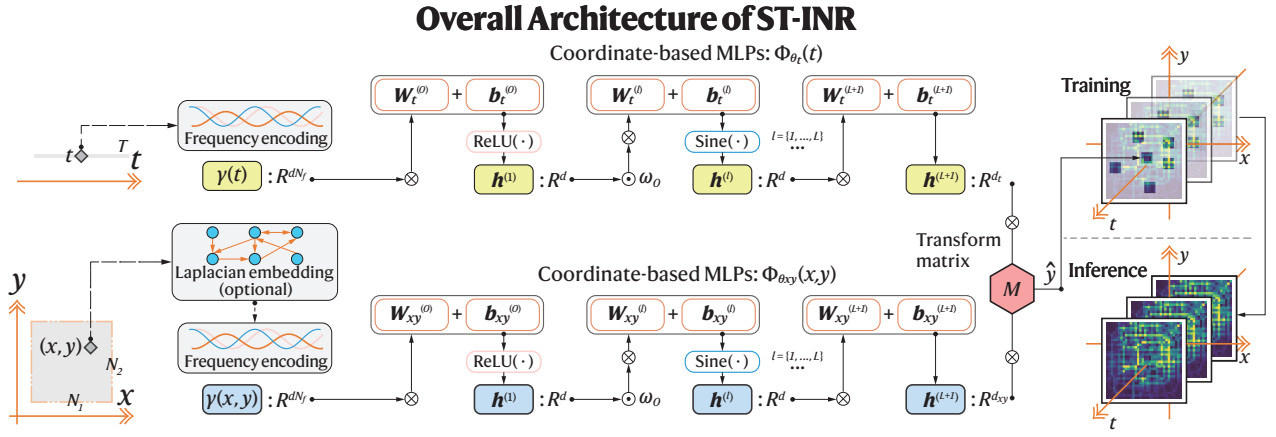


Figure 2: Overall architecture of the proposed ST-INR model (three-dimensional case).

### 3.1. Generalized traffic data learner through implicit neural representation

STTD usually exhibits explicit patterns, e.g., the temporal dynamics of traffic time series can show continuity, periodicity, and nonstationarity. However, the collected real-world traffic data often shows complex regularities due to undesirable observational conditions. It often suffers from sparse and noisy data, contains anomalies, and can be partially measured. To understand and exploit STTD to characterize traffic, practitioners resort to data-driven models to learn, reconstruct, denoise, analyze, and forecast partially observed STTD.

Generally, STTD can be generated from a complex process involving their locations in space and time domain. For instance, vehicle trajectories are defined by  $x - t$  coordinates. Origin-destination flows include both the  $x - y$  locations and the time point  $t$ . Sensor-based time series is associated with their relational position and time interval. On top of this understanding, the traffic dynamics are assumed to obey a system of equations:

$$\mathcal{F}(\mathbf{x}, \Phi, \nabla_{\mathbf{x}} \Phi, \nabla_{\mathbf{x}}^2 \Phi, \dots) = 0, \quad (1)$$

where  $\mathbf{x}$  is the spatial (or spatial-temporal) coordinates of the input domain, and the function  $\Phi : \mathbf{x} \mapsto \Phi(\mathbf{x})$  maps the coordinates to some quantities of interest, such as the traffic states at some spatiotemporal points. Since  $\Phi$  is defined by the constraint  $\mathcal{F}$  (which possibly contains the derivatives), it is *implicitly* modeled and usually parameterized by a deep neural network  $\Phi_{\theta}$  (Sitzmann et al., 2020). As a result,  $\Phi_{\theta}$  defines the implicit neural representation (INR) to approximate the explicit solution to Eq. (1). Given the true quantity  $f(\mathbf{x})$  at any location, INR can serve as a data-driven **learner** that can model the regularities of various traffic data by minimizing the continuous loss function in the entire definition space:

$$\min_{\theta} \mathcal{L} = \int_{\mathcal{D}} \|\mathcal{F}(f(\mathbf{x}), \Phi_{\theta}, \nabla_{\mathbf{x}} \Phi_{\theta}, \nabla_{\mathbf{x}}^2 \Phi_{\theta}, \dots)\| d\mathbf{x}, \quad (2)$$

where  $\mathcal{D}$  is the definition domain of  $\mathbf{x}$ . Due to its differentiable property, Eq. (2) can be optimized by the gradient descent method. With the spatiotemporal context, the learning problems of STTD on observed training data can be instantiated as a special form of Eq. (2) parameterized by  $\theta \in \Theta$ :

$$\min_{\theta} \mathcal{L}(\Omega(\Phi_{\theta}(\mathbf{x}, \mathbf{t})), \mathbf{y}) + \lambda \mathcal{R}(\Phi_{\theta}(\mathbf{x}, \mathbf{t})), \quad (3)$$

where  $\Phi_{\theta} : \mathcal{X} \subseteq \mathbb{R}^{N_x} \times \mathcal{T} \subseteq \mathbb{R}^{N_t} \mapsto \mathbb{R}^{D_{\text{out}}}$  is the implicit mapping function, i.e., the spatiotemporal learner,  $\mathbf{x} \in \mathcal{X}$ ,  $\mathbf{t} \in \mathcal{T}$  are the space-time coordinates,  $\mathbf{y} \in \mathbb{R}^{D_{\text{out}}}$  is the observation that can be partially measured or noisy,  $\Omega$  is a sampling operator,  $\mathcal{R}(\cdot)$  is a regularization defined on the continuous space to impose some priors over  $\Phi_{\theta}$ , and  $\lambda$  is the weight hyperparameter. Importantly, we treat STTD as a vector field and its regularities can be controlled by some underlying partial differential equations. Therefore, its state at an arbitrary location  $x$  and time  $t$  is subject to both spatial and temporal coordinates. For discrete problems, the definition domains can be discrete sets, e.g.,  $\mathcal{X} = \{0, 1, 2, \dots\}$ . For continuous problems, a continuous domain is considered, e.g.,  $\mathcal{T} \in \mathbb{R}^+$ .

In conventional low-rank models, Eq. (3) is instantiated by two components. The reconstruction loss  $\mathcal{L}$  is implemented by the approximation errors of matrix factorization or a surrogate nuclear norm minimization. The regularization term  $\mathcal{R}$  is formulated as an explicit penalty function such as total variation, graph Laplacian, and kernel function. In this work, we model them in a unified way by imposing implicit structures of regularization learned from data, which makes our method model-agnostic and adaptive for different patterns.

Drawing inspiration from INRs, we let multi-layer perceptrons (MLPs) be the parameterization  $\theta$ . With the universal approximation theorem, MLPs with infinite depth can theoretically fit arbitrary continuous functions

(Hornik, 1991). Concretely, taking the two-dimensional STTD as an example, the function representation is expressed as a continuous mapping from  $(x, t)$  coordinates to traffic state variables:

$$\begin{aligned}\Phi_\theta(x, t) &: (x, t) \mapsto \text{CoordMLP}(x, t) \in \mathbb{R}^{D_{\text{out}}}, \\ \text{CoordMLP}(x, t) &= \mathbf{W}^{(L+1)}(\phi^{(L)} \circ \phi^{(L-1)} \circ \dots \circ \phi^{(0)})([x, t]) + \mathbf{b}^{(L+1)}, \\ \mathbf{x}^{(\ell+1)} &= \phi^{(\ell)}(\mathbf{x}^{(\ell)}) = \sigma(\mathbf{W}^{(\ell)}\mathbf{x}^{(\ell)} + \mathbf{b}^{(\ell)}),\end{aligned}\quad (4)$$

where  $\text{CoordMLP}$  is the coordinate-based MLPs (Sitzmann et al., 2020),  $\mathbf{x}^{(\ell)}$  is the layerwise input with  $\mathbf{x}^{(0)} = [x, t]$ ,  $\sigma$  is the elementwise activation function, and  $\theta = \{\mathbf{W}^{(\ell)}, \mathbf{b}^{(\ell)} | \ell = 0, \dots, L\} \cup \{\mathbf{W}^{(L+1)}, \mathbf{b}^{(L+1)}\}$  are the model parameters need to be inferred. As an example, we can represent the speed field on regular mesh grid  $\mathbf{X} \in \mathbb{R}^{n \times t}$  with an INR  $\Phi_\theta(x, t) : \mathbb{R} \times \mathbb{R} \mapsto \mathbb{R}$  that satisfies  $\Phi_\theta(i, j) = \mathbf{X}[i, j], i \in \{0, 1, \dots, n\}, j \in \{0, 1, \dots, t\}$ . After learning the parameters, INR can predict the speed value at arbitrary coordinates  $(x, t) \in \mathbb{R} \times \mathbb{R}$ , even beyond the original discrete grid  $[i, j]$ .

### 3.2. Encoding high-frequency components in function representation

Low-rank models such as MF focus mainly on the utilization of low-frequency components. They assume that the reconstruction is dominated by a small number of modes. However, we argue that although STTD shows dominating patterns, high-frequency components can encode complex details and structures about STTD. Especially, high-frequency parts can relate with significant local patterns (Sen et al., 2019). Nevertheless, learning the high-frequency tails of the spectrum is a longstanding challenge for machine learning methods. The famous *frequency principle* revealed by Fourier analysis indicates that deep neural networks tend to fit low-frequency components during model training (Xu et al., 2019). This is understood as the ‘‘spectral bias’’ of deep neural networks (Rahaman et al., 2019). To alleviate this spectral bias, we adopt two advanced techniques to learn high-frequency components. We first denote the spatial-temporal input coordinate as  $\mathbf{v} = (x, t) \subseteq \mathbb{R} \times \mathbb{R}^+$ .

The first strategy is to equip  $\text{CoordMLP}$  with periodic activation functions (Sitzmann et al., 2020):

$$\phi_s^{(\ell)}(\mathbf{v}^{(\ell)}) = \sin(\omega_0 \cdot \mathbf{W}^{(\ell)}\mathbf{v}^{(\ell)} + \mathbf{b}^{(\ell)}), \ell = \{1, \dots, L\}, \quad (5)$$

where  $\omega_0$  is a frequency factor to ensure the sin function spans multiple periods over  $[-1, 1]$ , and the weights are initialized as  $\mathbf{w}_i^{(\ell)} \in \mathbb{R}^D \sim \mathcal{U}(-\sqrt{6/d}, \sqrt{6/d})$  to have a standard deviation of 1 (Sitzmann et al., 2020). The sine activation introduces periodicity to the hidden states and its gradient is also a sine function everywhere, which makes the neural networks easily learn complicated patterns.

The second solution is to use concatenated random Fourier features (CRF) in the input layer (Tancik et al., 2020; Benbarka et al., 2022). We can select problem-specific Fourier features and incorporate them into the input of  $\text{CoordMLP}$ . However, obtaining a predefined frequency can be challenging due to the complex patterns of STTD. Therefore, unlike the original method in (Tancik et al., 2020; Benbarka et al., 2022), we employ a series of CRF with different scales in the input layer to explicitly inject the high-frequency components:

$$\gamma(\mathbf{v}) = [\sin(2\pi\mathbf{B}_1\mathbf{v}), \cos(2\pi\mathbf{B}_1\mathbf{v}), \dots, \sin(2\pi\mathbf{B}_{N_f}\mathbf{v}), \cos(2\pi\mathbf{B}_{N_f}\mathbf{v})]^\top \in \mathbb{R}^{d_{N_f}}, \quad (6)$$

where the Fourier basis frequency  $\mathbf{B}_k \in \mathbb{R}^{d/2 \times c_{\text{in}}}$  are sampled from Gaussian distribution  $\mathcal{N}(0, \sigma_k^2)$ . By setting a large number of frequency features  $N_f$  and a series of scale parameters  $\{\sigma_k^2\}_{k=1}^{N_f}$ , we can sample a variety of frequency patterns in the input domain, which is crucial for the reconstruction of complex patterns (see Section 5.1). In addition, having diverse frequency features enables our model to be adaptive to different input data, simplifying the process of selecting a specific frequency values. The rationale of using Fourier feature mapping can be explained by the theory of neural tangent kernel (NTK). Tancik et al. (2020) show that CRF can transform the effective NTK into a stationary kernel with a tunable bandwidth, enabling faster convergence for high-frequency components.

The overall workflow of a single frequency-enhanced  $\text{CoordMLP} : \hat{\mathbf{y}} = \Phi_\theta(\mathbf{v})$  can be formulated as follows:

$$\begin{aligned}\mathbf{h}^{(1)} &= \text{ReLU}(\mathbf{W}^{(0)}\gamma(\mathbf{v}) + \mathbf{b}^{(0)}), \\ \mathbf{h}^{(\ell+1)} &= \phi_s^{(\ell)}(\mathbf{h}^{(\ell)}) = \sin(\omega_0 \cdot \mathbf{W}^{(\ell)}\mathbf{h}^{(\ell)} + \mathbf{b}^{(\ell)}), \ell = \{1, \dots, L\}, \\ \hat{\mathbf{y}} &= \mathbf{W}^{(L+1)}\mathbf{h}^{(L+1)} + \mathbf{b}^{(L+1)},\end{aligned}\quad (7)$$

where  $\mathbf{W}^{(\ell)} \in \mathbb{R}^{d_{(\ell)} \times d_{(\ell+1)}}$ ,  $\mathbf{b}^{(\ell)} \in \mathbb{R}^{d_{(\ell+1)}}$  are layerwise parameters, and  $\hat{\mathbf{y}} \in \mathbb{R}^{d_{\text{out}}}$  is the predicted value. The combination of these two strategies achieves high-frequency low-dimensional regression, empowering the coordinate-based MLPs to learn complex details with high resolution.

### 3.3. Factorizing spatial-temporal variability through coordinate disentanglement

Using a single  $\Phi_\theta$  to model entangled spatial-temporal interactions within a continuous domain can be challenging. Therefore, we decompose the spatiotemporal process into separate variables in two dimensions using coordinate disentanglement. Specifically, we factorize the definition domain of  $\Phi_\theta$  into two axes:

$$\begin{aligned}\Phi_\theta(\mathbf{v}) &= \Phi_{\theta_x}(x)\mathbf{M}_{xt}\Phi_{\theta_t}(t)^\top, \\ \Phi_{\theta_x} : \mathcal{X} &\mapsto \mathbb{R}, x \mapsto \Phi_{\theta_x}(x) \in \mathbb{R}^{d_x}, \\ \Phi_{\theta_t} : \mathcal{T} &\mapsto \mathbb{R}, t \mapsto \Phi_{\theta_t}(t) \in \mathbb{R}^{d_t},\end{aligned}\tag{8}$$

where  $\Phi_{\theta_x}$  and  $\Phi_{\theta_t}$  are defined by Eq. (7). To further align the two components, which can have different dimensions and frequency patterns, we adopt a middle transform matrix  $\mathbf{M}_{xt} \in \mathbb{R}^{d_x \times d_t}$  to model their interactions in the hidden manifold. This formulation makes Eq. (8) a generalized and continuous matrix factorization model. When the spatial-temporal coordinates  $x$  and  $t$  are defined on a discrete grid, a sampled matrix  $\mathbf{Y}$  can be given as  $\{\mathbf{Y}[i, j] = \Phi_{\theta_x}(x^{(i)})\Phi_{\theta_t}(t^{(j)})^\top, \forall i, j \in \mathbb{N}_+\}$ , which intrinsically constructs a discrete matrix factorization model. On the contrary, it can process data or functions that exist beyond the regular mesh grid of matrices, capturing complex spatiotemporal patterns using the expressive power of deep learning.

In practice, we can set  $d_x = d_t = d_{xt}$  as the hidden dimension.  $\mathbf{M}_{xt}$  is learned at the same time as other parameters in  $\Phi_{\theta_x}$  and  $\Phi_{\theta_t}$  and we find that initializing it as an identity matrix can result in a good nontrivial solution. A significant difference between our model and existing low-rank models is that we adopt a large factorization dimension, i.e., the hidden dimension  $d_{xt}$ , to ensure the learning of a wider singular spectrum while at the same time encouraging a low-rank solution through the **implicit low-rank regularization** brought by gradient descent (Arora et al., 2019). Important discussions about the two hidden dimensions are provided in Section 3.6.2. It is also noteworthy that in this factorized formulation, the temporal and spatial components can adopt different frequency features, thereby learning different implicit mappings to encode complex data patterns. This coordinate disentanglement strategy also brings efficiency benefits (see Section 3.6.4).

### 3.4. Learning traffic data in arbitrary domains

The mapping  $\Phi_\theta$  enables us to parameterize the function spaces over traffic data. With this powerful and flexible tool, we seek to learn a wide range of traffic data, such as individual trajectory, sensor-based time series, dynamic origin-destination flow, and network traffic state, as a continuous function  $\Phi_\theta$ . However, in reality, traffic data can be sampled and stored in an irregular way. For example, a sensor network can be abstracted as a weighted directed graph where vertices denote detectors of the network, and edges indicate the connectivity (reachability) between sensors. In the Euclidean case, we already know the regularity of the data domain, e.g.,  $\mathcal{X}, \mathcal{T} \subseteq \mathbb{R}$ , and INRs can be readily trained on a discrete sampling of a signal over a regular lattice. However, when there are traffic data on an arbitrary topological space  $\mathcal{H}$ , instead of a regular lattice such as the  $x-t$  coordinate, we cannot represent  $\mathcal{H}$  in a canonical coordinate system. To ease the difficulty, we assume that we can obtain a discrete graph realization  $\mathcal{G}$  sampled from the unknown topological space of the continuous signal. We then approach the non-Euclidean data modeling problem by projecting it to the Laplacian eigenvector space.

Specifically, in this generalized setting, we consider a graph signal  $f : \mathcal{H} \mapsto \mathcal{Y}$  with its discrete graph realization  $\mathcal{G}(V, E, \mathbf{A})$ . The basic elements are node set  $V = \{v_i | i = 1, \dots, n\}$ , edge set  $E \subseteq V \times V$  and weighted adjacency matrix  $\mathbf{A} \in \mathbb{R}^{n \times n}$  (undirected). We resort to the graph spectral embedding technique (Grattarola and Vandergheynst, 2022), bypassing the need to know the continuous space underlying the traffic graph signals. Since the graph describes the relations between graph signals, we can obtain a meaningful coordinate system by manipulating the spectral embedding of the graph Laplacian (Grattarola and Vandergheynst, 2022). Given the adjacency matrix  $\mathbf{A}$ , the symmetric normalized Laplacian as well as its eigendecomposition are given as:

$$\mathbf{L}_s = \mathbf{I} - \mathbf{D}^{-\frac{1}{2}}\mathbf{A}\mathbf{D}^{-\frac{1}{2}} = \mathbf{U}^\top \text{diag}(\lambda_1, \dots, \lambda_n)\mathbf{U},\tag{9}$$

where  $\mathbf{D} = \text{diag}(\sum_{i'} a_{ii'})$  is the degree matrix,  $\mathbf{U}$  is the matrix whose column is the eigenvectors and the eigenvalues are ordered as  $\lambda_1 \leq \lambda_2 \leq \dots, \lambda_n$ . Correspondingly, the associated eigenvectors form an orthonormal basis  $\{\mathbf{u}_j \in \mathbb{R}^n, j = 1, \dots, n\}$ , which is treated as the coordinate in the Laplacian eigenspace for each node  $v_j$ :

$$\mathbf{e}_j = [u_{1,j}, u_{2,j}, \dots, u_{n,j}]^\top \in \mathbb{R}^n.\tag{10}$$

In practice, we truncate the first  $k$  values as the final embedding  $\tilde{\mathbf{e}}_j[:k] \in \mathbb{R}^k$  to reduce complexity. Similar to the routine of regular INRs, a neural network  $\Phi_\theta : \tilde{\mathbf{e}}_j \mapsto f(v_j)$  is trained to map the spectral embedding of each node (coordinate in the Laplacian eigenspace) to the graph signal value. After model training, we can calculate the corresponding spectral embedding to infer the graph signal values for any node, as long as we can sample from the discrete graphs. Note that eigenvectors of the graph Laplacian are a discrete approximation of the continuous eigenfunctions of the Laplace operator on  $\mathcal{H}$  (Ortega et al., 2018), which forms a natural extension from the input in the Euclidean domain to the non-Euclidean domain. Importantly, if the signals are defined on spatiotemporal graphs, such as sensor-based time series, it can also be transformed into a vertex-time factorization formulation, just as Eq. (8).

**Algorithm 1:** Spatiotemporal implicit neural representations of traffic data

---

**Input:** Network parameter  $\theta$ , partially measured dataset  $\mathcal{D} = \{(\mathbf{v}_i, \mathbf{y}_i)\}_{i=1}^M$ .  
**Output:** Trained ST-INR model  $\Phi_\theta$  and the predictions at queried coordinates  $\{\hat{\mathbf{y}}_i\}_{i=1}^{M^*}$ .

// Model training stage

- 1 Initialize  $\Phi_{\theta_r}, \forall r \in \{1 \dots n_{c_{in}}\}$  and the transform tensor  $\mathcal{M}$ ;
- 2 Sample the basis frequency matrices  $\mathbf{B}_k \sim \mathcal{N}(0, \sigma_k^2), \forall k \in \{1, \dots, N_f\}$ ;
- 3 **while** not convergence **do**
- 4     Sample a batch  $\mathcal{B}$  of data pairs  $\{(\mathbf{v}_j, \mathbf{y}_j)\}_{j \in \mathcal{B}, \mathcal{B} \subseteq \mathcal{D}}$ ;
- 5     // Forward process
- 6     **for**  $i \in \mathcal{B}$  **do**
- 7          $\Phi_\theta(\mathbf{v}_i) \leftarrow \mathcal{M} \times_1 \Phi_{\theta_1}(v_1) \times_2 \dots \times_{c_{in}} \Phi_{\theta_{c_{in}}}(v_{c_{in}})$ ;
- 8         // Gradient descent for updating parameters
- 9          $\theta \leftarrow \theta - \eta \nabla_\theta \frac{1}{|\mathcal{B}|} \sum_{i \in \mathcal{B}} \|\mathbf{y}_i - \Phi_\theta(\mathbf{v}_i)\|_2^2$ ;
- 10     // Model inference stage
- 11 Evaluate  $\Phi_\theta$  at given queried coordinates within the definition domain  $\{\mathbf{v}_i^*\}_{i \in M^*}$ ;
- 12 **for**  $i \in M^*$  **do**
- 13      $\hat{\mathbf{y}}_i \leftarrow \Phi_\theta(\hat{\mathbf{v}}_i^*) \leftarrow \mathcal{M} \times_1 \Phi_{\theta_1}(v_1^*) \times_2 \dots \times_{c_{in}} \Phi_{\theta_{c_{in}}}(v_{c_{in}}^*)$ ;

---

### 3.5. High-dimensional extensions and gradient-based optimization

Eq. (8) describes the two-dimensional case that can model an arbitrarily spatial-temporal traffic data matrix. For higher-dimensional structures, such as the time-varying origin-destination flows and grid-based traffic states, we can represent them in an expanded formulation. Taking inspiration from (Luo et al., 2023), we can organize the multidimensional data into a generalized Tucker tensor (Kolda and Bader, 2009) format. Different from the conventional Tucker model defined on discrete grids, ST-INR are fully defined on continuous input domains and the factor matrices are parameterized by INRs. Specifically, given a single input-output data pair  $(\mathbf{v}, \mathbf{y})$  where  $\mathbf{v} \in \mathbb{R}^{c_{in}}$  is the  $c_{in}$  dimensional input coordinate and  $\mathbf{y} \in \mathbb{R}^{c_{out}}$  is the corresponding true data value. The ST-INR model for high-dimensional data can be formulated as:

$$\begin{aligned} \Phi_\theta(\mathbf{v}) &= \mathcal{M} \times_1 \Phi_{\theta_1}(v_1) \times_2 \dots \times_{c_{in}} \Phi_{\theta_{c_{in}}}(v_{c_{in}}), \forall (v_1, v_2, \dots, v_{c_{in}}) \in \mathbf{v}, \\ \Phi_{\theta_i} : v_i &\mapsto \Phi_{\theta_i}(v_i) \in \mathbb{R}^{n_i}, \forall i \in \{1, \dots, c_{in}\}, \end{aligned} \quad (11)$$

where  $\mathcal{M} \in \mathbb{R}^{n_1 \times \dots \times n_{c_{in}}}$  is the core tensor, and  $\theta = \{\theta_1, \theta_2, \dots, \theta_{c_{in}}\} \cup \mathcal{M}$  are the model parameters. Similarly, each  $\Phi_{\theta_i}$  can be defined on a topological space with different base frequencies. The factorized size  $n_i$  can also be full-dimensional, as described in Section 3.3.

Given a data instance, for example, a bounded spatiotemporal speed contour, we can sample a set containing  $M$  collocation pairs  $\mathcal{D} = \{(\mathbf{v}_i, \mathbf{y}_i)\}_{i=1}^M$  where  $\mathbf{v}_i \in \mathbb{R}^{c_{in}}$  is the input coordinate and  $\mathbf{y}_i \in \mathbb{R}^{c_{out}}$  is the true data value. For example, if the speed contour has  $N$  space grids and  $T$  time points, then we have  $M = NT$ ,  $c_{in} = 2$ , and  $c_{out} = 1$ . Given training data  $\mathbf{x}$  and the model  $\Phi_\theta$ , we can evaluate  $\Phi_\theta$  in Eq. (11) at all collocation points. Then Eq. (3) can be instantiated in the following form:

$$\min_{\theta} \mathcal{L}(\theta; \mathcal{D}) = \frac{1}{M} \sum_{i=1}^M \|\mathbf{y}_i - \Phi_\theta(\mathbf{v}_i)\|_2^2. \quad (12)$$

Note that the regularization  $\mathcal{R}$  in Eq. (3) is learned implicitly from the data instance, rather than an explicit penalty term. We will highlight the benefits of implicit regularization in Section 3.6.

The above equation is fully differentiable, we can optimize it using gradient-based optimizer, i.e.,

$$\theta_{k+1} \leftarrow \theta_k - \eta \nabla_\theta \mathcal{L}(\theta, \{(\mathbf{v}_j, \mathbf{y}_j)\}_{j \in \mathcal{B}, \mathcal{B} \subseteq \mathcal{D}}) |_{\theta=\theta_k}, \quad (13)$$

where  $k$  is the gradient step,  $\eta$  is the learning rate, and  $\mathcal{B}$  is the data batch. More advanced optimizers such as Adam can also be adopted. Notably, we will discuss the benefits of gradient descent over Eq. (12) in Section 3.6.2.

In summary, the overall workflow of ST-INR are shown in Algorithm 1.

### 3.6. Theoretical Analysis

In addition to the data learning power of the proposed model, this section presents several salient features that are important for real-world traffic data applications, including *encoding of high-frequency structures*, *implicit low-rank regularization*, *inherent smoothness*, and *reduced complexity*. The proposed ST-INR explicitly encodes high-frequency structures to learn complex details of various STTD while at the same time implicitly learning low-rank and smooth priors from data to reconstruct the dominating modes.



### 3.6.1. High frequency encodings

The key rationale for INRs is the exploitation of high-frequency structures in data signals. Based on the theory of neural tangent kernel (NTK) (Jacot et al., 2018; Tancik et al., 2020), we first indicate that the Fourier features in Eq. (6) introduce a composed NTK that is beneficial for the convergence of neural networks to high-frequency components, providing a solution to the spectral bias of standard MLPs.

**Lemma 1** (Neural network dynamics through NTK (Jacot et al., 2018)). *Let  $f$  become a deep neural network with parameters  $\theta$ , the training dynamics of it can be approximated by the NTK defined as:  $k_{\text{NTK}}(\mathbf{x}_i, \mathbf{x}_j) = \mathbb{E}_{\theta} \langle \frac{\partial f(\mathbf{x}_i; \theta)}{\partial \theta}, \frac{\partial f(\mathbf{x}_j; \theta)}{\partial \theta} \rangle$ . When considering the input in a hypersphere, the NTK reduces to a dot product kernel  $k_{\text{NTK}}(\mathbf{x}_i, \mathbf{x}_j) = h_{\text{NTK}}(\mathbf{x}_i^T \mathbf{x}_j)$ . Then for a MLP trained with an L2 loss and a learning rate  $\eta$ , the network's output for test data  $\mathbf{X}_{\text{test}}$  after  $t$  steps of training on a training dataset  $\{\mathbf{X}, \mathbf{y}\}$  can be approximated as:*

$$\hat{\mathbf{y}}^{(t)} = f(\mathbf{X}_{\text{test}}; \theta) \approx \mathbf{K}_{\text{test}} \mathbf{K}^{-1} (\mathbf{I} - e^{-\eta \mathbf{K} t}) \mathbf{y}, \quad (14)$$

where  $\mathbf{K}$  is the kernel matrix between all data pairs of training data with  $k_{i,j} = k_{\text{NTK}}(\mathbf{x}_i, \mathbf{x}_j)$ , and  $\mathbf{K}_{\text{test}}$  is the NTK matrix between all pairs of testing data. On top of this approximation, we are interested in the behaviors of model in training convergence. Consider the eigendecomposition  $\mathbf{K} = \mathbf{Q} \mathbf{\Lambda} \mathbf{Q}^T$ , the projected absolute error of training loss is given by:

$$|\mathbf{Q}^T (\hat{\mathbf{y}}_{\text{train}}^{(t)} - \mathbf{y})| \approx |\mathbf{Q}^T ((\mathbf{I} - e^{-\eta \mathbf{K} t}) \mathbf{y} - \mathbf{y})| = |e^{-\eta \mathbf{\Lambda} t} \mathbf{Q}^T \mathbf{y}|. \quad (15)$$

This indicates that the absolute training loss will decrease approximately exponentially at the rate  $\eta \lambda$ , where the larger eigenvalues will be fitted faster than those smaller ones. A kernel with rapidly decaying spectrum fails to converge to high-frequency components. Instead, a wider kernel with slower spectral attenuation can achieve easier convergence.

*Proof.* The proof can be found in Jacot et al. (2018).  $\square$

The above lemma states that a standard MLP is difficult to fit high-frequency components, and we can control the spectral bias of deep neural networks through manipulating the kernel to cover a relatively wide spectrum. This is achieved by the CRF in Eq. (6) with the following lemma.

**Lemma 2** (Composing NTK with Fourier features (Tancik et al., 2020)). *Given the Fourier mapping in Eq. (6), the induced NTK has the form:*

$$k_{\gamma}(\gamma(\mathbf{v}_1), \gamma(\mathbf{v}_2)) = \gamma(\mathbf{v}_1)^T \gamma(\mathbf{v}_2) = \sum_{j=1}^{N_f} \cos(2\pi \mathbf{B}_j (\mathbf{v}_1 - \mathbf{v}_2)) \triangleq h_{\gamma}(\mathbf{v}_1 - \mathbf{v}_2), \quad (16)$$

which is a shift-invariant kernel, a.k.a., stationary kernel. Then the CRF passed through a MLP activates a composed NTK:

$$h_{\text{NTK}}(\mathbf{x}_i^T \mathbf{x}_j) = h_{\text{NTK}}(\gamma(\mathbf{v}_1)^T \gamma(\mathbf{v}_2)) = h_{\text{NTK}}(h_{\gamma}(\mathbf{v}_1 - \mathbf{v}_2)). \quad (17)$$

This result means that Fourier feature mapping of the input coordinates makes the composed NTK stationary, serving as a convolution kernel over the input domain (Tancik et al., 2020).

This lemma shows that CRF transforms a kernel from the dot product into a composed stationary one:  $k(\gamma(\mathbf{u}), \gamma(\mathbf{v})) = h(\gamma(\mathbf{u})^T \gamma(\mathbf{v})) = h \circ \gamma(\mathbf{u} - \mathbf{v})$ , making it better suited for low-dimensional regression. Notably, regression with a stationary kernel corresponds to data reconstruction with a convolution filter.

Combining lemmas 1 and 2, we see that higher frequency mapping results in a composed kernel with a wider spectrum, allowing faster convergence for high-frequency patterns. By adding a wide range of Fourier features to the input mapping, the resulting composed kernel can have a wider spectrum, serving as an effective convolutional filter for signal reconstruction. In fact, the model predictions generated by Eq. (17) are sums of observed points, weighted by a function of the Euclidean distance, which is demonstrated to be effective for traffic data reconstruction problems, such as the adaptive smoothing method (Treiber and Kesting, 2013).

Next, we show that the MLP layers with sine activation functions in Eq. (5) are also equivalent to Fourier mappings, thus showing similar effects as the CRF. The following lemma explains this equivalence.

**Lemma 3** (The equivalence between periodic activation and Fourier features). *Given the input coordinate  $\mathbf{v} \in \mathbb{R}^{d_{in}}$ , a two-layer MLP with sine activation function and weights  $\mathbf{W}_f \in \mathbb{R}^{2N_d \times d_{in}}$ ,  $\mathbf{W} \in \mathbb{R}^{d \times 2N_d}$  is formed as:*

$$\phi_s(\mathbf{v}) = \mathbf{W} \sin(\omega \mathbf{W}_f \mathbf{v} + \mathbf{b}_f) + \mathbf{b}, \quad (18)$$

then it can be equivalent to a single-layer linear network with a series of Fourier mapped inputs:

$$h_f(\mathbf{v}) = \mathbf{W} [\cos(2\pi \mathbf{W}_{f_1} \mathbf{v}), \sin(2\pi \mathbf{W}_{f_1} \mathbf{v}), \dots, \cos(2\pi \mathbf{W}_{f_N} \mathbf{v}), \sin(2\pi \mathbf{W}_{f_N} \mathbf{v})] + \mathbf{b}. \quad (19)$$

*Proof.* We prove this lemma by construction. Without generality, we denote:  $\mathbf{W}_f = [\mathbf{W}_{f_1}, \mathbf{W}_{f_1}, \dots, \mathbf{W}_{f_N}, \mathbf{W}_{f_N}]^\top \in \mathbb{R}^{2Nd \times d_{in}}$  with  $\mathbf{W}_{f_i} \in \mathbb{R}^{d \times d_{in}}$  and  $\mathbf{b}_f = [\pi/2, 0, \dots, \pi/2, 0] \in \mathbb{R}^{2Nd}$ . Then Eq. (18) can be rewritten as:

$$\mathbf{W} \sin(\omega \begin{bmatrix} \mathbf{W}_{f_1} \mathbf{v}, \\ \mathbf{W}_{f_1} \mathbf{v}, \\ \vdots \\ \mathbf{W}_{f_N} \mathbf{v}, \\ \mathbf{W}_{f_N} \mathbf{v} \end{bmatrix} + \begin{bmatrix} \pi/2, \\ 0, \\ \vdots \\ \pi/2, \\ 0 \end{bmatrix}) + \mathbf{b} = \mathbf{W} \begin{bmatrix} \cos(\omega \mathbf{W}_{f_1} \mathbf{v}), \\ \sin(\omega \mathbf{W}_{f_1} \mathbf{v}), \\ \vdots \\ \cos(\omega \mathbf{W}_{f_N} \mathbf{v}), \\ \sin(\omega \mathbf{W}_{f_N} \mathbf{v}), \end{bmatrix} + \mathbf{b}. \quad (20)$$

When  $\omega = 2\pi$ , the above equation equals (19).  $\square$

The two techniques show similar effects in both the input and hidden layers of ST-INR and enable it to encode high-frequency structures adaptively to learn complex data patterns, which is a significant superiority over standard low-rank models.

### 3.6.2. Implicit low-rank regularization

In addition to high-frequency details, STTD is dominated by a few low-rank structures (Tan et al., 2013; Asif et al., 2016). Conventional low-rank models such as matrix factorization and nuclear norm minimization capture the low-rank structures with explicit low-rank constraints. As an alternative, we show that our model features an implicit low-rank regularization that is learned from the gradient descent over the target data.

Recall that  $d_x$  and  $d_t$  in Eq. (8) determines the dimension of the interaction between spatial and temporal factors. In canonical matrix factorization or tensor factorization methods, such a dimension is set to a very small number  $r \ll \min\{N, T\}$  with  $N, T$  denoting the dimension of the input matrix, to encourage a low-rank solution. It is widely acknowledged in the field that low-rankness significantly benefits the reconstruction of traffic data (Tan et al., 2013). However, the set  $d_x = d_t = r$  can restrict the model expressivity of  $\Phi_x(x)$  and  $\Phi_t(t)$  that are parameterized by deep neural networks. A compromise needs to be reached between explicit low-rank regularization and high model capacity. Additionally, traffic data from different sources and scales can have distinct low-rank patterns. For example, the low-rank pattern identified in microscopic data such as vehicle trajectory can not generalize to macroscopic data such as mobility flow. The determination of different rank values for various STTD can pose a great challenge.

Fortunately, we can address this issue by the implicit low-rank regularization of deep models. Specifically, we treat our model as a special case of deep matrix factorization (DMF) (Arora et al., 2019). We can ensure both the low-rankness and model capacity by adopting a full-dimensional factor matrix, i.e.,  $d_x = d_t = \min\{N, T\}$  and imposing an implicit low-rank regularization from the gradient descent method.

To analyze the low-rankness of our model, on the one hand, we can impose some structural constraints on Eq. (8). We characterize  $\Phi$  as a dynamical system that is conditioned on the evolution step  $\tau$  of gradient descent. We assume  $\Phi_x(\tau) \in \mathbb{R}^{N \times \min\{N, T\}}$ ,  $\Phi_t(\tau) \in \mathbb{R}^{T \times \min\{N, T\}}$  have orthonormal columns and  $\mathbf{M}(\tau) \in \mathbb{R}^{\min\{N, T\} \times \min\{N, T\}}$  is diagonal. Then  $\Phi(\tau) = \Phi_x(\tau) \text{diag}(\sigma_1(\tau), \dots, \sigma_{\min\{N, T\}}(\tau)) \Phi_t(\tau)^\top$  with  $\sigma_j(\tau)$  denotes the signed singular values of  $\Phi(\tau)$ . On the other hand, if we omit the activation and bias terms, we have  $\Phi(\mathbf{v}) = \mathbf{W}_x^{L+1} \mathbf{W}_x^L \dots \mathbf{W}_x^0 \mathbf{v} \mathbf{M} \mathbf{W}_t^{0, \top} \dots \mathbf{W}_t^{L+1, \top}$ , which forms a special DMF model defined in (Arora et al., 2019). Under these conditions, our factorized model invokes the following lemma.

**Lemma 4** (Implicit low-rank regularization of DMF (Arora et al., 2019)). *Given the loss function  $\mathcal{L}$  in Eq. (12), the signed singular values  $\sigma(\tau)$  of  $\Phi_\tau$  evolve by the following rule:*

$$\dot{\sigma}_j(\tau) = -2L(\sigma_j^2(\tau))^{1-\frac{1}{2L}} \langle \nabla \mathcal{L}, \Phi_x^j(\tau) \Phi_t^j(\tau)^\top \rangle, \quad j = 1, \dots, \min\{N, T\}, \quad (21)$$

where  $\Phi_x^j(\tau)$ ,  $\Phi_t^j(\tau)$  are the  $j$ -th column vectors of  $\Phi_x$ ,  $\Phi_t$ , and  $L$  is the depth of `CoordMLP`.

*Proof.* The proof can be found in Theorem 3 of Arora et al. (2019).  $\square$

Lemma 4 indicates that the evolution of singular values of  $\Phi$  conditions on the depth  $L$  of the factorized model. When  $L \geq 1$ , the nontrivial factor  $-2L(\sigma_j^2(\tau))^{1-\frac{1}{2L}}$  intensifies the evolution of large singular values and attenuates that of smaller ones. Such an updating rule promotes a factorization that features a small number of large singular values and a large number of small ones. In addition, a larger  $L$  encourages more significant gaps between large and small singular values. This is an implicit bias (regularization) towards a low-rankness. With this, we can ensure the expressivity of MLPs by setting a large width and depth and obtain a low-rank resolution by the regularization of gradient descent. Moreover, we can directly adopt full-dimensional factorization to bypass the need to select a task-specific rank  $r$ . Demonstrations of this property are given in Section 5.4.

### 3.6.3. Inherent smoothness from MLPs

Apart from the low-rankness, some other structural priors also have significant impacts on STTD. For example, smoothness priors are essential to reconstruct traffic data under poor observation conditions (Chen et al., 2022; Nie et al., 2023b). As revealed in previous work, temporal smoothness (continuity) is helpful for estimating data from missing time intervals, and graph spectral or spatial smoothness can be exploited for extrapolation. However, most of these handcrafted priors are task-dependent and may not be generalized to other scenarios. Therefore, we resort to the inherent smoothness property of our model that is scenario-independent and fully learned from the data. Specifically, Luo et al. (2023) has shown that, under some assumptions, the tensor function is Lipschitz continuous in Euclidean space. As a complement, we examine its continuity in arbitrary spectral domain, i.e., in a topological space defined in Section 3.4.

**Lemma 5** (Spectral smoothness of ST-INR). *Consider a single ST-INR defined on an arbitrary topological space:  $\Phi(\mathbf{e}) = \mathbf{W}^L(\sigma(\mathbf{W}^{(L-1)}(\dots\sigma(\mathbf{W}^1\mathbf{e})))$ ), we assume that the  $\ell_1$  norm of each INR weight matrix  $\mathbf{W}^{(\ell)}$  is bounded by  $\xi$ , and the  $\ell_1$  norm of middle transform  $\mathcal{M}$  is bounded by  $\eta$ , then we have:*

$$\begin{aligned} |\Phi(\mathbf{e}_1, \mathbf{e}_2, \dots, \mathbf{e}_n) - \Phi(\mathbf{e}'_1, \mathbf{e}_2, \dots, \mathbf{e}_n)| &\leq \eta\xi^{nL}\delta^{n-1}|\mathbf{e}_1 - \mathbf{e}'_1|, \\ |\Phi(\mathbf{e}_1, \mathbf{e}_2, \dots, \mathbf{e}_n) - \Phi(\mathbf{e}_1, \mathbf{e}'_2, \dots, \mathbf{e}_n)| &\leq \eta\xi^{nL}\delta^{n-1}|\mathbf{e}_2 - \mathbf{e}'_2|, \\ &\vdots \\ |\Phi(\mathbf{e}_1, \mathbf{e}_2, \dots, \mathbf{e}_n) - \Phi(\mathbf{e}_1, \mathbf{e}_2, \dots, \mathbf{e}'_n)| &\leq \eta\xi^{nL}\delta^{n-1}|\mathbf{e}_n - \mathbf{e}'_n|, \end{aligned} \quad (22)$$

which means that  $\Phi(\mathbf{e})$  is Lipschitz continuous in an arbitrary spectral coordinate system  $\mathbf{e}$ .

*Proof.* According to the factorization rule in Eq. (8), we have  $\Phi(\mathbf{e}_1, \mathbf{e}_2, \dots, \mathbf{e}_n) = \mathcal{M} \times_1 \Phi(\mathbf{e}_1) \times_2 \Phi(\mathbf{e}_2) \cdots \times_n \Phi(\mathbf{e}_n)$ , where  $\times_n$  is the tensor product (Kolda and Bader, 2009). For  $\forall \Phi(\mathbf{e})$ ,  $|\Phi(\mathbf{e})| \leq |\mathbf{W}^L| |\sigma(\mathbf{W}^{L-1} \cdots \sigma(\mathbf{W}^1))| |\mathbf{e}|$ , and both  $\sin(\cdot)$  and  $\text{ReLU}(\cdot)$  are Lipschitz continuous everywhere with Lipschitz constant equals to 1, then it holds:

$$\begin{aligned} |\Phi(\mathbf{e}_1, \mathbf{e}_2, \dots, \mathbf{e}_n) - \Phi(\mathbf{e}'_1, \mathbf{e}_2, \dots, \mathbf{e}_n)| &= |\mathcal{M} \times_1 (\Phi(\mathbf{e}'_1) - \Phi(\mathbf{e}_1)) \times_2 \Phi(\mathbf{e}_2) \cdots \times_n \Phi(\mathbf{e}_n)|, \\ &\leq \eta\xi^{(n-1)L} \prod_{i \neq 1} |\mathbf{e}_i| |\Phi(\mathbf{e}'_1) - \Phi(\mathbf{e}_1)|, \\ &\leq \eta\xi^{nL} \prod_{i \neq 1} |\mathbf{e}_i| |\mathbf{e}'_1 - \mathbf{e}_1|. \end{aligned} \quad (23)$$

Eq. (23) holds for  $n$  coordinates. If we let  $\delta = \max\{|\mathbf{e}_i|, i = 1, \dots, n\}$ , Eq. (22) naturally holds.  $\square$

Lemma 5 indicates that our model is continuity in arbitrary spectral coordinate system. This property enables our model to impose smoothness priors on graphs and beyond the regular  $x - t$  coordinates, which aligns with the characteristics of network-wide traffic data. We illustrate this feature in Section 4.3. With this property, we can implicitly regularize the smoothness of the solution through governing the continuity of MLPs, without having to elaborate on a complicated penalty function. In practice, this can be achieved by controlling the weight decay parameters of MLPs, refer to Section 5.3.

### 3.6.4. Reduced computational complexity

Due to the factorized design, our model features reduced computational complexity. Besides, it does not require resolution-dependent quadratic or cubic storage, such as the factor matrix and the core tensor, in low-rank models. This makes it applicable for learning large-scale traffic data instance. We examine the complexity of each forward pass in two input settings: (1) continuous domain and (2) regular grids.

For case (1), we consider that  $n$  observation points in a two-dimensional space are measured for training. The model inputs two separate coordinates  $[n, 1] \times [n, 1]$  and maps each of them to  $[n, d]$  where  $d$  is the output size. Then two factors are merged to compute the final output  $[n, 1]$ . In this situation, the time complexity of a  $L$  layer ST-INR with hidden size  $D$  is  $\mathcal{O}(nLD^2 + nd^2 + nDd)$ .

For case (2), the input is a mesh grid with size  $n_1 \times n_2$ . Without factorization, the complexity becomes  $\mathcal{O}(n_1n_2LD^2 + n_1n_2d^2 + n_1n_2Dd)$ . When spatial-temporal distanglement is adopted, the complexity reduces to  $\mathcal{O}((n_1 + n_2)LD^2 + (n_1 + n_2)Dd)$ , which is much more efficient for large-scale data with  $n_1 + n_2 \ll n_1n_2$ .

As for space complexity, general MF models need to store the entire factor matrices  $\mathbf{U} \in \mathbb{R}^{n_1 \times d}$ ,  $\mathbf{V} \in \mathbb{R}^{n_2 \times d}$  and in the running memory to update each iteration. Instead, our model only needs to store some weight matrix after model training, e.g.,  $\mathbf{W}_1 \in \mathbb{R}^{1 \times D}$ ,  $\mathbf{W}_L \in \mathbb{R}^{D \times d}$ , which is agnostic to the input dimensions, which makes our model scalable for large input dimensions.

We will show the computational superiority of our factorization strategy in Section 5.2.

## 4. Demonstrations of Different Applications

This section demonstrates the practical effectiveness of the proposed ST-INR model. Several experiments were carefully designed on public STTD datasets, covering scales ranging from highway corridors, urban grids,

to network levels. We first compare it with some representative low-rank models on benchmark tasks, then we perform supplementary studies to highlight the unique properties of our model. All experiments are conducted on a computing platform with a single NVIDIA GeForce RTX A6000 GPU (48 GB). **PyTorch implementations of this project will be publicly available at: [https://github.com/tongnie/traffic\\_dynamics](https://github.com/tongnie/traffic_dynamics).**

#### 4.1. Corridor-level application: Highway traffic state estimation

We first consider the traffic state estimation (TSE) problem in highway corridors. TSE is a prerequisite procedure for accurate reconstruction of individual trajectories (Chen et al., 2024). Traditional methods include traffic flow models such as the Lighthill-Whitham-Richards model and smoothing-based models such as the adaptive smoothing method (Treiber and Kesting, 2013). Actually, if we organize the spatial-temporal speed field into regular meshes, this can be treated as a structured matrix completion problem (Wang et al., 2023).

We adopt the trajectory data from NGSIM, US 101 dataset<sup>1</sup> for experiment. To create the TSE problem, we select an area in the second lane with a length of 1500 ft and a time span of 2600 s. Two input scenarios are considered: (a) estimation from discrete mesh grids; (b) estimation from continuous trajectories. In the first setting, we need to split the continuous spatial-temporal domain into regular mesh grids, to ensure the function of discrete baselines. Therefore, we use a time resolution of 5 s and a space resolution of 7 ft, resulting in a matrix of dimension (215, 520). We consider the following baselines: (1) Matrix factorization with alternating least squares (MF); (2) Low-rank matrix completion based on nuclear norm minimization (LRMC); (3) Laplacian convolutional representation-based matrix completion (LCR) (Chen et al., 2022); (4) Circulant nuclear norm minimization model (CircNNM) (Liu and Zhang, 2022); (5) STHTC: spatiotemporal Hankelized tensor completion (Wang et al., 2023), which is a state-of-the-art TSE model; (6) ASM: Adaptive smoothing method (Treiber and Kesting, 2013); (7) MLP: vanilla MLP model. We randomly sampled 15% of the trajectories as observed probe vehicles, and all models need to estimate the full speed field. The input to ST-INR is the discrete index of each observed cell, and the observed trajectory points are used for supervision. Then the trained ST-INR are adopted to predict the traffic states at all meshes.

Table 1: Results (in terms of WMAPE, RMSE, and MAE) of highway traffic state estimation on mesh grid.

Metric	ST-INR	MF	LRMC	LCR	CircNNM	STHTC	ASM	MLP
WMAPE	<b>11.05%</b>	21.70%	20.60%	12.21%	12.72%	12.06%	13.57%	29.29%
RMSE (ft/s)	<b>4.88</b>	9.96	9.62	5.48	5.74	5.46	5.94	12.51
MAE (ft/s)	<b>3.71</b>	7.29	6.92	4.10	4.27	4.05	4.56	9.84

Best performances are bold marked.

Results on discrete grids are given in Tab. 1 and Fig. 3. As can be seen, our model outperforms competing models by a large margin in this benchmark task. As indicated in Fig. 3 (especially the black box in the lower right corner), our model can reconstruct fine details with high resolution, which is more consistent with the real congestion shock wave. Interestingly, the vanilla MLP fails to learn any congestion wave and approximates the average speed distribution. This result clearly demonstrates that the high-quality reconstruction by ST-INR can be ascribed to the utilization of high-frequency features.

In the second scenario, we evaluate our model directly on continuous trajectory points, in which all existing low-rank baselines are incapable of working. We randomly sampled 10% of the  $(x, t)$  coordinates as the collocation points to fit the continuous mapping, leading to approximately 5 thousands of points. The input to ST-INR is a set of  $(x, t)$  coordinates. We compare our model with a MLP model equipped with sine activation function (Sitzmann et al., 2020). It is noteworthy that after being trained on the sampled collocation points, INRs can make inference at any resolution and position. Therefore, we upsample the trajectory points with a higher resolution. We uniformly sample 1600 points along the time axis and 800 points along the location axis, resulting in a  $245 \times$  upsampling rate. As shown in Fig. 4, our model can generate a consistent speed contour and successfully reconstruct the traffic flow phenomena, e.g., the shockwave propagation and the free-flow speed.

#### 4.2. Grid-level application: Urban mesh-based flow estimation

The second task evaluates the estimation of the urban mesh-based flow map. This task can have wide applications in measuring and regulating mobility flow in urban areas (Liang et al., 2019). The grid flow map can be arranged with two spatial dimensions to denote the locations of the grid or origin-destination locations, and with a temporal dimension to denote the time. This structure can be processed by a third-order tensor.

Two public datasets are adopted: (1) TaxiBJ<sup>2</sup>: grid-based taxi volume records in the main district of Beijing at a 30-min interval from March 1 to June 30, 2015. We keep the first 7 days and use the spatial resolutions of

<sup>1</sup><https://www.fhwa.dot.gov/publications/research/operations/07030/index.cfm>.

<sup>2</sup><https://github.com/yoshall/UrbanFM>.



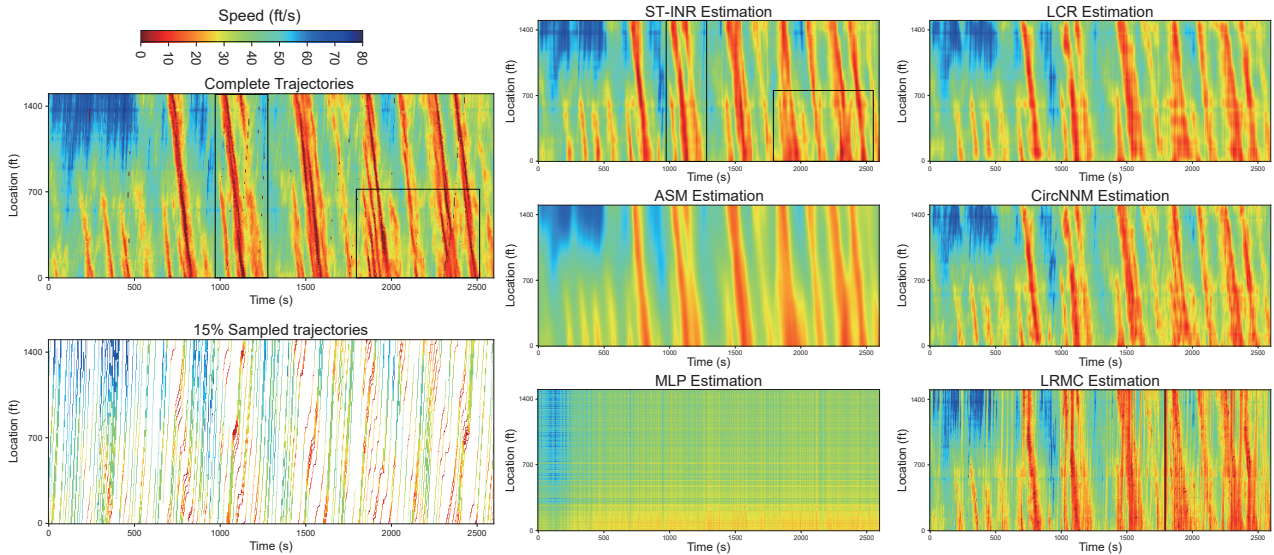


Figure 3: TSE performances on discrete grid.

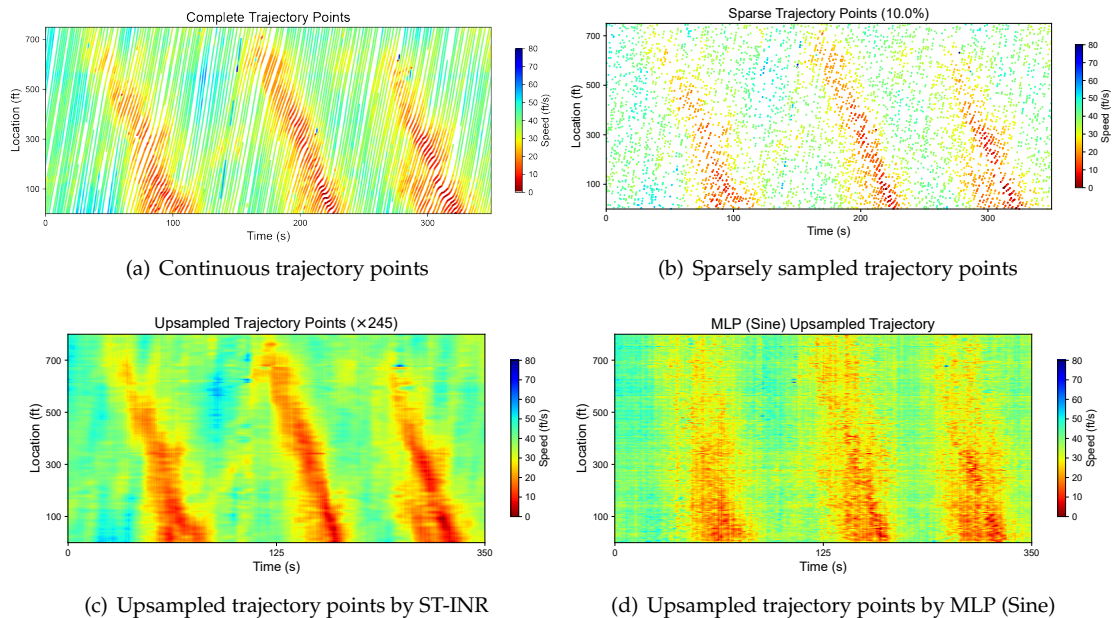


Figure 4: TSE performances on continuous space.

$32 \times 32$  and  $64 \times 64$ , resulting in tensors with sizes  $(336, 32, 32)$  and  $(336, 128, 128)$ ; (2) TaxiNYC<sup>3</sup>: taxi trip records in NYC. Similarly to previous work, we use 69 zones in Manhattan district as pick-up and drop-off zones. We aggregate the daily taxi trip into origin-destination matrix and concatenate the mobility data from January to May in 2020 to form a tensor of size  $(69, 69, 151)$ . Due to the impact of COVID-19, there is a drastic drop in travel demands after March 2020 (see the first row in Fig. 6). For TaxiBJ data, we train separate models to estimate volumes at different resolutions. We use 20% of the data as observed flow and train all models to predict the remaining volumes. For TaxiNYC data, due to the sparsity of origin-destination flows, we randomly sample 40% of the mobility data as training data. For baselines, we consider: (1) CP: Canonical polyadic tensor decomposition; (2) Tucker: Tucker tensor decomposition; (3) LATC: Low-rank autoregressive tensor completion (Chen et al., 2021b), which is a state-of-the-art model for tensor-structured time series data; (4) LRTC-TNN: low-rank tensor completion based on truncated tensor nuclear norm (Chen et al., 2020); (5) Vanilla MLP model.

Qualitative and quantitative results are given in Tab. 2 and Figs. 5 and 6. First, Tab. 2 shows that our mode significantly surpasses other baselines, even without explicit temporal modules such as the autoregression. Note that ST-INR depends on the absolute locations of the data points, which is beneficial for the estimation of location-dependent flow patterns. Second, by observing Fig. 5, we find that ST-INR can capture the main

<sup>3</sup><https://www.nyc.gov/site/tlc/about/tlc-trip-record-data.page>.

shape of the Beijing road network and perform well in both resolutions. While tensor-based models can generate blur estimations without distinguishing the background area. MLPs cannot complete this task because of the inability to learn high-frequency patterns. Finally, Fig. 6 compares the results of ST-INR and the tensor model on NYC data. Clearly, our model readily learns complex mobility patterns, but the Tucker model can have difficulty learning accurate flows in many zones. In addition, due to the sparsity of mobility flows, tensor-based models can overfit zero values and generate incorrect flows for zones with small values.

Table 2: Results of urban grid flow map estimation.

Metric		ST-INR	CP	Tucker	LATC	LRTC-TNN	MLP
TaxiBJ $32 \times 32$	RMSE (veh/30min)	<b>62.11</b>	95.86	96.35	77.17	73.27	237.86
	WMAPE	<b>14.93%</b>	24.43%	24.23%	17.40%	16.79%	55.83%
TaxiBJ $64 \times 64$	RMSE (veh/30min)	<b>21.64</b>	33.06	32.45	27.35	26.62	98.77
	WMAPE	<b>17.44%</b>	29.15%	28.80%	22.51%	22.34%	74.71%
TaxiNYC	RMSE (veh/d)	<b>8.71</b>	15.34	15.23	11.25	12.10	62.86
	WMAPE	<b>14.53%</b>	22.28%	21.24%	16.87%	17.28%	70.22%

Best performances are bold marked.

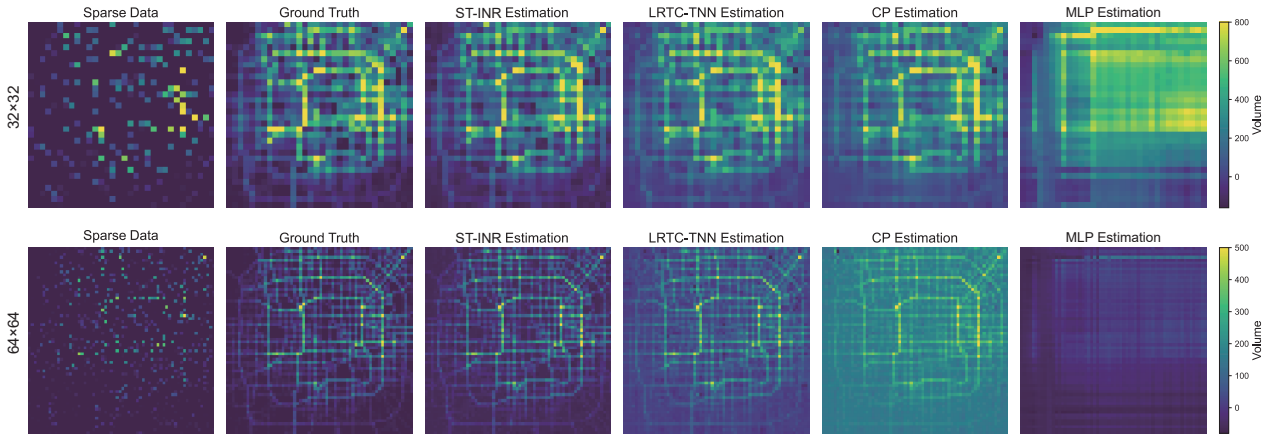


Figure 5: Model performances on TaxiBJ data (the 10-th snapshot).

#### 4.3. Network-level application: Highway and urban network state estimation

Next, we focus on estimating the states of traffic on the entire road network. The real-time states of the road network are vital for network-wide control and analysis (Saeedmanesh et al., 2021; Paipuri et al., 2021). Unlike the above data structures, network data can sometimes be organized as a graph. Therefore, it is challenging for models that are defined on Euclidean space to model non-Euclidean data. In this case, we use the method in Section 3.4 to project the input coordinates to the Laplacian space. We use two variations of ST-INR with respect to the definition space, including: ST-INR (L): ST-INR defined in Laplacian eigenvector space, and ST-INR (E): ST-INR defined in Euclidean space. We train both of them to predict the adopted data.

For highway sensor network, we adopt: (1) PeMS-BAY: highway loop speed data from 325 static detectors in the San Francisco South Bay Area collected by the Caltrans Performance Measurement System (PeMS) in 5 minutes<sup>5</sup>, where the first 30 days of data are used in our experiment; and (2) Seattle: speed data collected by 323 loop detectors deployed on freeways in Seattle area<sup>6</sup>. We also use a month of data in a 5-min interval. For urban road network, we consider the Chicago and Berlin network from the NeurIPS2021-traffic4cast Competition<sup>7</sup>, which transforms link-based traffic speed values to gray values and organizes the network states at each time into an “image” with size (495, 436). We adopt 288 frames to consider the within-day variations.

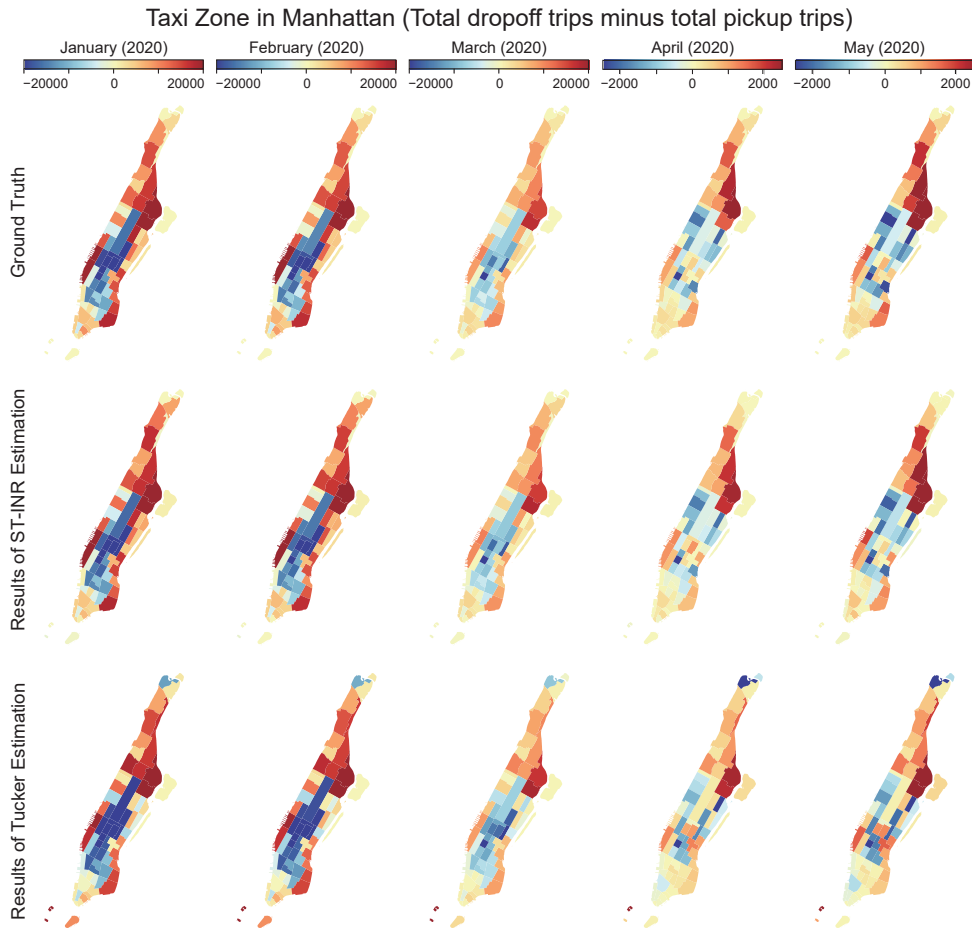
We create a “missing sensor” estimation problem for the two highway datasets. This task aims to estimate the speed at locations without loop sensors, which is viewed as a spatial kriging problem in the literature (Wu et al., 2021; Nie et al., 2023b). We randomly remove a proportion of sensors (60% for PEMS-BAY and 80% for

<sup>4</sup>The visualization of this figure is based on the code from: <https://github.com/xinychen/vars>.

<sup>5</sup><https://pems.dot.ca.gov/>.

<sup>6</sup><https://github.com/zhuyongc/Seattle-Loop-Data>.

<sup>7</sup><https://developer.here.com/sample-data>.

Figure 6: Model performances on TaxiNYC data (Jan.-May., 2020).<sup>4</sup>

Seattle) as unmeasured and train models to predict the unmeasured speed values using the adjacency between the sensors. To compare with methods capable of performing this task, we adopt baselines that are regularized either by graphs or smoothness priors: (1) SMF: smooth matrix factorization with total variation penalty (He et al., 2015); (2) GRALS: graph-regularized alternating least squares (Rao et al., 2015); (3) LCR; (4) GLTL: greedy low-rank tensor learning with Laplacian regularization (Bahadori et al., 2014); (5) FP: a state-of-the-art graph diffusion-based model to estimate missing graph labels, called feature propagation (Rossi et al., 2022). The results of model comparison are shown in Tab. 3 and Fig. 7.

Table 3: Results of highway network-wide traffic state estimation.

Metric		ST-INR (L)	ST-INR (E)	SMF	GRALS	LCR	GLTL	FP
PEMS-BAY	RMSE (km/h)	<b>6.99</b>	9.49	8.74	9.86	8.44	11.45	10.28
	WMAPE	<b>6.94%</b>	9.00%	9.17%	7.76%	8.92%	10.88%	7.61%
	MAE (km/h)	<b>4.34</b>	5.63	5.74	4.86	5.59	6.81	4.77
Seattle	RMSE (km/h)	8.51	<b>7.14</b>	9.36	7.57	8.02	8.82	7.64
	WMAPE	9.47%	<b>7.81%</b>	11.41%	8.43%	9.67%	11.26%	8.23%
	MAE (km/h)	5.46	<b>4.49</b>	6.58	4.86	5.57	6.49	4.73

Best performances are bold marked.

It is demonstrated that ST-INR can be generalized to different coordinate systems (input spaces). For PEMS-BAY data with more complex graph structures, the Laplacian embedding plays a more important role in refining the input coordinates. In addition, because of the inherent smoothness property derived from the MLP, ST-INR can generate smooth estimations on both regular lattice and spectral embedding, even without any explicit smoothness or graph regularization terms. This finding echoes our analysis in Section 3.6.3. Combined with the excellent capability of encoding high-frequency patterns, ST-INR can produce more realistic reconstruction than other baselines. Conversely, smoothness regularization on Euclidean space does not achieve good performance on non-Euclidean space, such as the results of LCR and SMF in Fig. 7 (b).



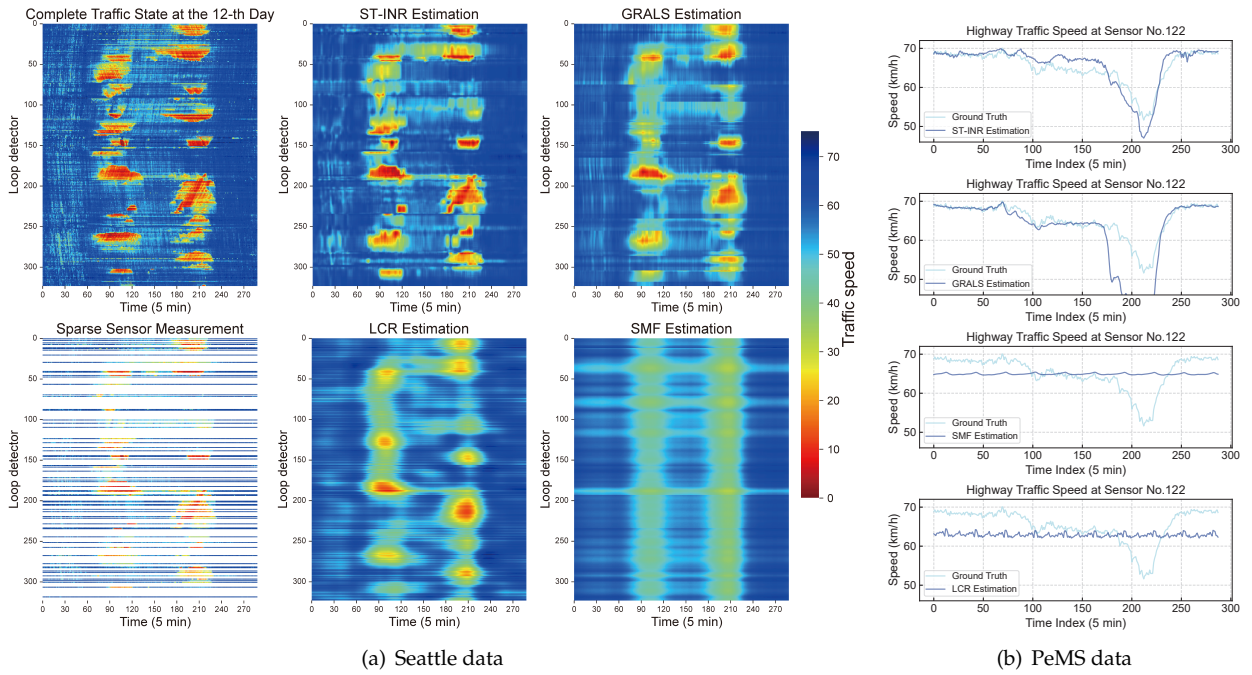


Figure 7: Model performances on Seattle and PEMS-BAY speed data.

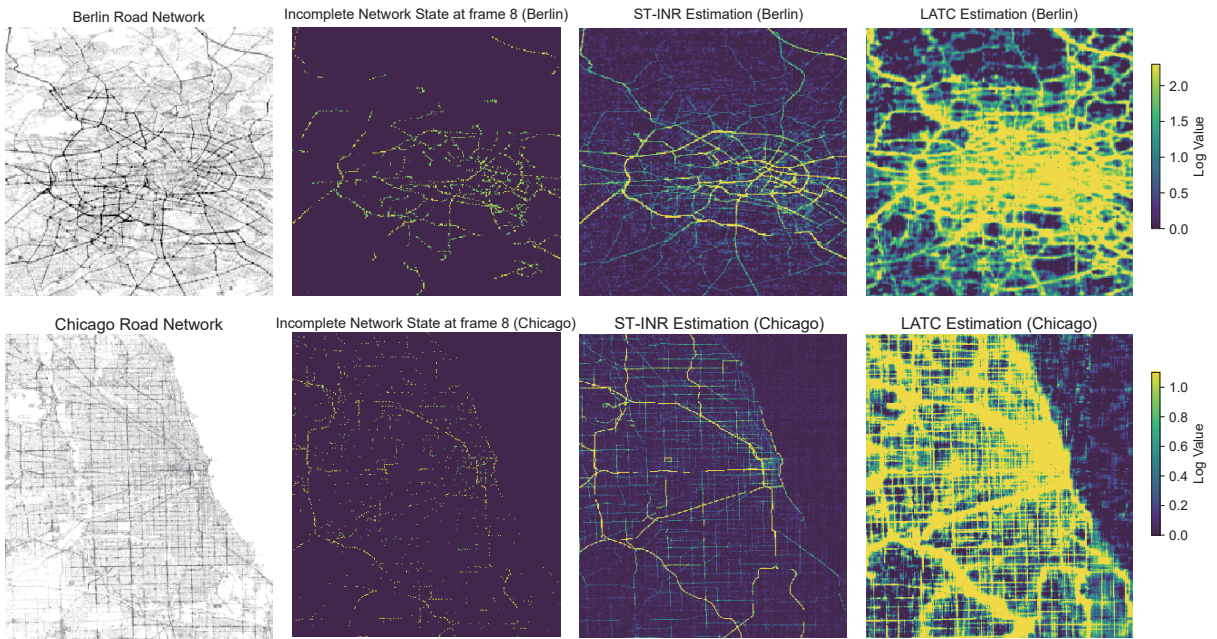


Figure 8: Model performances on Chicago and Berlin network.

The case of urban network is more challenging due to the complexity of urban road network. As a result, we randomly select 50% of the raw data as observations. This task requires the model to learn high-frequency patterns to reconstruct the complexity of urban road network. To evaluate, we train ST-INR on each of the Berlin and Chicago networks and compare it with state-of-the-art tensor completion model LATC. Fig. 8 reveals some surprising findings. First, ST-INR can successfully recover the complex network topology, as well as the traffic states, even without the guidance of the network topology. Second, pure low-rank models are incapable of learning these data with complicated topological structures, which again verifies the significance of high-frequency components. Our model encodes a wide range of high-frequency series in the input layer, thereby being adaptive to different frequency patterns in real-world traffic data.

## 5. Algorithmic analysis

On top of the analysis in Section 3.6 and the experimental results in Section 4, this section provides more discussions on the properties of our model to examine how these properties contribute to the learning of STTD.



### 5.1. Frequency analysis

Compared to vanilla MLPs and low-rank models, ST-INR can capture high-frequency patterns within natural signals. In other words, the incorporation of high-frequency information benefits the learning of ST-INR. We indicate this property by examining the Fourier spectrum and the convergence behaviors during training. The Fourier spectrum in Fig. 9 (a) shows that ST-INR can utilize high-frequency encodings to model meaningful frequency details in real data. Compared to pure low-rank matrix factorization, it preserves more energy in the back part of the spectrum. Fig. 9 (b) compares the loss curves under different frequency settings. After gradually increasing the frequency encoding from 0 to 10, the model achieves a lower training loss, which means that it becomes easier to fit the real-world data with higher frequencies.

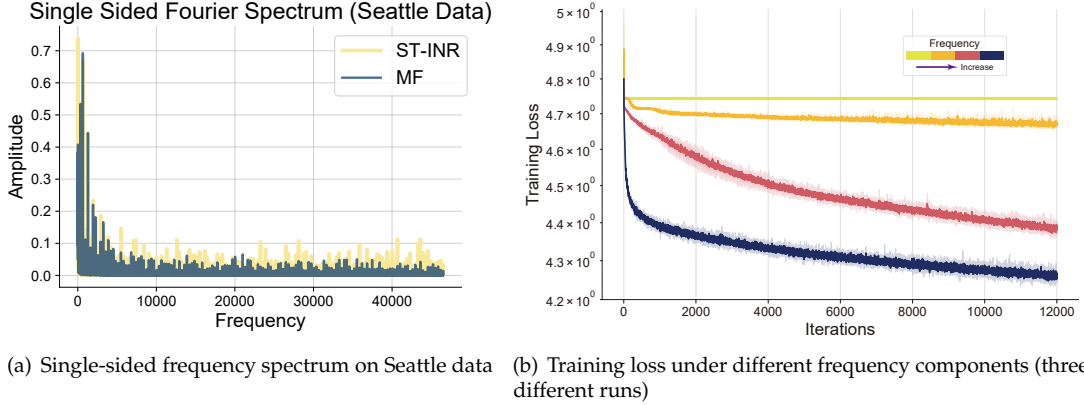


Figure 9: Frequency analysis.

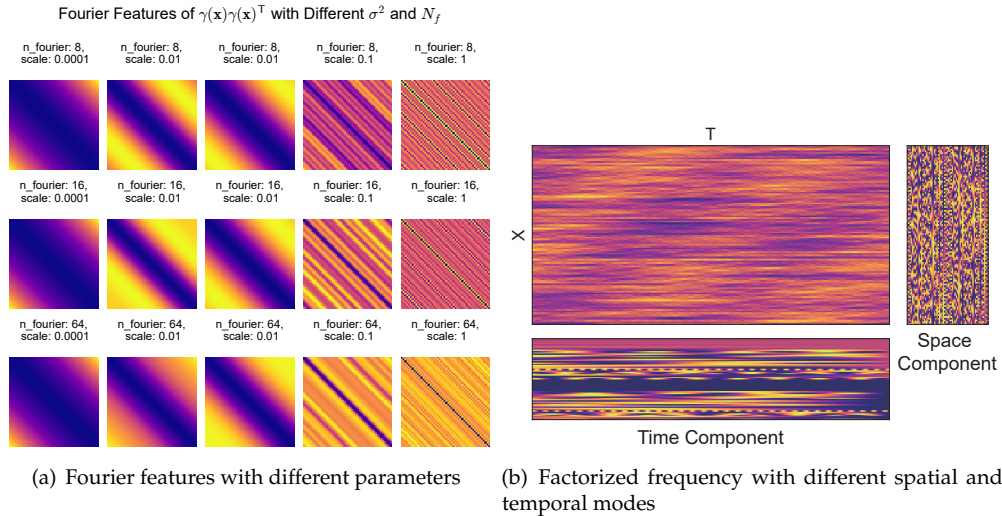


Figure 10: Visualization of random Fourier features.

Note that the CRF in Eq. (6) has two important parameters, i.e., the number of Fourier features  $N_f$  and the dictionary of scales  $\{\sigma_1^2, \dots, \sigma_{N_f}^2\}$ . We study its effect in Fig. 10. As can be seen, increasing the scales can have a wider spectrum, covering more frequency patterns, such as periodicity. All the while, adding the number of CRF can interpolate the frequency distributions, sharing more details. Moreover, thanks to the factorized design, we can use separate frequency encodings with different  $N_f$  and  $\sigma^2$  along the time and space dimensions.

### 5.2. Model efficiency

Since our model is optimized through stochastic gradient descent, it can be efficiently implemented by a modern deep learning framework such as PyTorch. Besides, due to the spatial-temporal factorization, it features reduced computational complexity. We adopt TaxiBJ data with different data scales (from  $8 \times 8$  to  $128 \times 128$ ) to examine its efficiency in Fig. 11. All measurements are performed on a single GPU device. As indicated by our analysis in Section 3.6.4, the full mode has cubic complexity with respect to the spatial (temporal) dimension  $n$ . In contrast, the factorized version approximates to scale linearly to the dimensions, which is consistent with the results in Fig. 11. This scalability makes our model feasible for large-scale datasets.

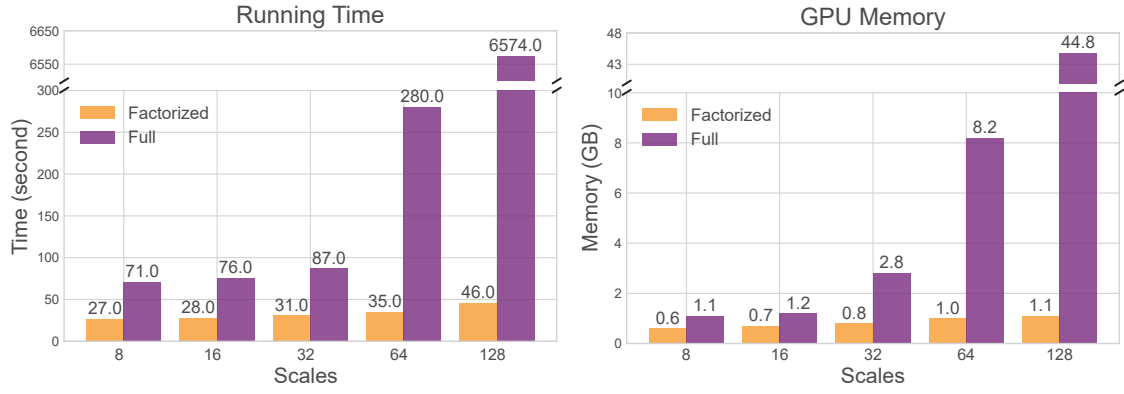


Figure 11: Model efficiency on TaxiBJ data.

### 5.3. Hyperparameter analysis

As a deep neural network model, it has a number of parameters that need to be tuned. As suggested by [Luo et al. \(2023\)](#), the weight decay parameter has an impact on overall continuity, thus affecting the smoothness regularization. Furthermore, deep neural networks are supposed to benefit from the model depth ([He et al., 2016](#)). We evaluate the two hyperparameters in several adopted datasets in Fig. 12. We can see that adding more INR layers indeed benefits the model performance, but increases the risks of overfitting on small datasets. For data with more perceivable details such as Seattle, using a too large smoothness penalty will make the model degrade. For data with relatively simpler patterns, such as TaxiBJ, more smooth solutions are encouraged. In practice, setting the decay parameter to 1 can yield a desirable performance on most of the data.

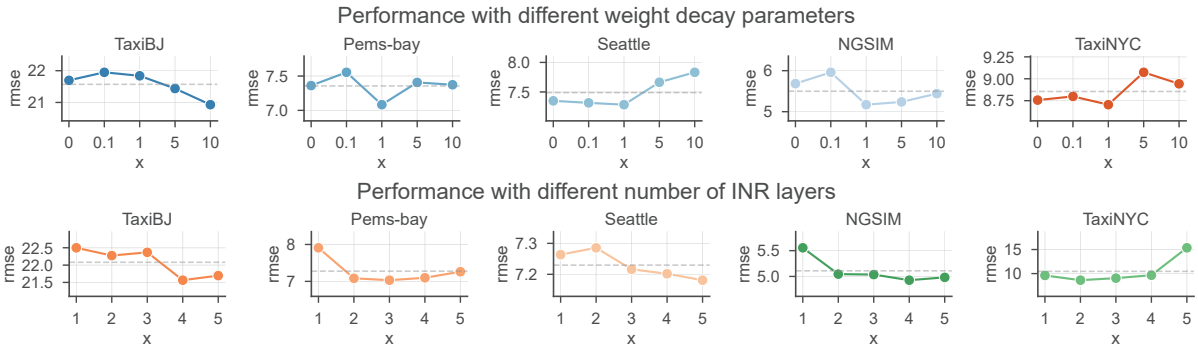


Figure 12: Hyperparameter studies on different datasets.

### 5.4. Implicit low-rank regularization

Low-rankness is a strong inductive bias for STTD, especially when the observations are sparse. The implicit low-rankness of our model is discussed in Section 3.6.2. We now provide some empirical evidence on this implicit regularization. To evaluate the rank (norm) minimization effect, we manually construct a rank-5 matrix by reconstructing NGSIM data using a truncated singular value decomposition, i.e.,  $\tilde{\mathbf{X}} = \mathbf{U}[:, : 5] \mathbf{D}[:, : 5] \mathbf{V}^T[:, : 5, :]$ . We then examine the nuclear norm and effective rank ([Roy and Vetterli, 2007](#)) of the estimations of different methods under different missing rates. As a reference, we add the result of a rank-constrained minimum nuclear norm as the global optima, termed “Nuclear Min” in Fig. 13 (a) and (b).

The results presented in Fig. 13 (a)-(b) indicate that as the missing rate increases, all methods converge towards a solution with lower rank and smaller nuclear norm. However, our model consistently achieves a lower norm and a smaller effective rank than other matrix completion methods. More importantly, although our model has much smaller nuclear norm than ground truth and global optimal values, it has close effective rank values to them. This reveals that our model does not rely on the minimization of a surrogate nuclear norm, but directly encourages a low-rank solution. This differentiates it from existing nuclear norm-based methods.

To further evaluate whether the dimension of factorization has impacts on the implicit low-rankness like the rank constraint on factor matrices of the MF model, we increase the dimension from  $r = 10$  to  $r = \min\{N, T\}$ .  $r = \min\{N, T\}$  results in a full-dimensional factorization. The results in Fig. 13 (c)-(d) are insightful: a low rank-constrained model fails to recover the true norm and rank values, leading to a underfitting resolution; Instead, with the gradual relaxation of the rank constraints, even the full-dimensional case can produce a precise reconstruction. This finding is in alignment with previous work ([Gunasekar et al., 2017](#)).

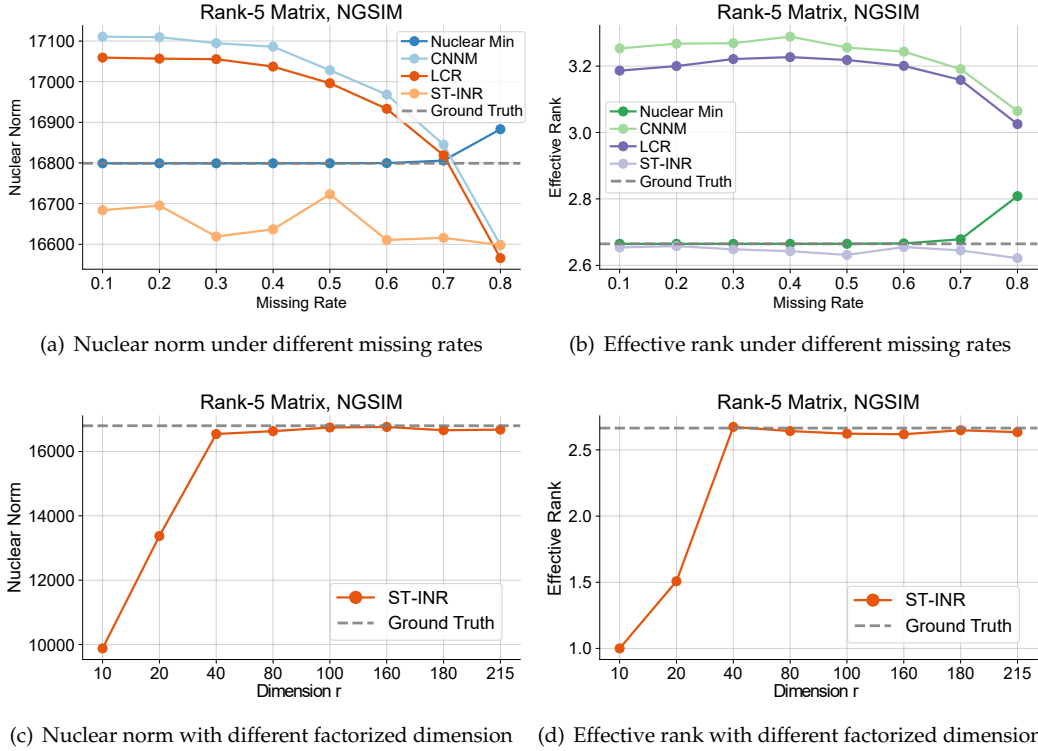


Figure 13: Implicit low-rank regularization on a rank-5 speed matrix of NGSIM data.

To summarize, the above empirical results suggest that our model has an implicit regularization that admits stronger bias towards low-rankness, which shows better performance than existing nuclear norm minimization methods. A desirable reconstruction can be achieved by using the implicit regularization of DMF in Section 3.6.2, without the need to elaborate on nuclear norm-based surrogate or perform rank-constrained alternating optimization. In addition, we can also bypass the need to tune the rank parameter  $r$  by directly using a full-dimensional factorization. These findings could inspire a new line for traffic data imputation or forecasting studies that adopt a newly designed norm or a variation of the nuclear norm optimized by ADMM or ALS.

## 6. Conclusion and outlook

In this work, we demonstrate a novel spatiotemporal traffic data (STTD) learning method based on implicit neural representations, termed ST-INR. By parameterizing STTD as continuous deep neural networks, we train ST-INR to directly map the spatial-temporal coordinates to the traffic states. ST-INR explicitly encodes high-frequency structures to learn complex details of STTD while at the same time implicitly learning low-rank priors and smoothness regularization from data itself to reconstruct dominant patterns. Due to the generality of this representation, it can be exploited to model a variety of STTD, such as vehicle trajectory, origin-destination flows, grid flows, highway sensor networks, and urban networks. Experimental results on various real-world benchmarks indicate that our model consistently outperforms traditional low-rank models such as tensor factorization and nuclear norm minimization. It also has the potential to generalize across different data structures and problem settings. In addition, other important properties such as the incorporation of high-frequency structures, implicit low-rankness, and inherent smoothness can function as new inductive biases for STTD modeling, providing an alternative to conventional low-rank models.

Meanwhile, based on our framework, there are still some directions that require future efforts, for example,

1. Physics-informed learning of traffic dynamics: How to enable the current framework to be guided by physics? A possibly feasible routine in integrating it with physics-based machine learning methods, such as physics-informed neural networks (Raissi et al., 2019).
2. Forecasting irregularly sampled traffic time series: Real-world traffic data may be recorded by sensors with different sampling frequencies or by varying the number of mobile sensors. Due to the continuous nature of our model, it is possible to adopt it to forecast irregular traffic data (Ye et al., 2012).
3. Representation learning of vehicle paths: How to organize vehicle path sets into an acceptable input format of INRs and perform path flow estimation for urban road networks is a promising question.

Overall, we believe that the proposed ST-INR can provide an opportunity to unify STTD learning methods and thereby facilitate the development of a large foundation model for generalized STTD analysis.

## Acknowledgement

This research was sponsored by the National Natural Science Foundation of China (52125208), the National Natural Science Foundation of China's Young Scientists Fund (52302413), the Science and Technology Commission of Shanghai Municipality (No. 22dz1203200), and the Research Grants Council of the Hong Kong Special Administrative Region, China (Project No. PolyU/25209221 and PolyU/15206322).

## References

- Arora, S., Cohen, N., Hu, W., Luo, Y., 2019. Implicit regularization in deep matrix factorization. *Advances in Neural Information Processing Systems* 32.
- Asif, M. T., Dauwels, J., Goh, C. Y., Oran, A., Fathi, E., Xu, M., Dhanya, M. M., Mitrovic, N., Jaillet, P., 2013. Spatiotemporal patterns in large-scale traffic speed prediction. *IEEE Transactions on Intelligent Transportation Systems* 15 (2), 794–804.
- Asif, M. T., Mitrovic, N., Dauwels, J., Jaillet, P., 2016. Matrix and tensor based methods for missing data estimation in large traffic networks. *IEEE Transactions on intelligent transportation systems* 17 (7), 1816–1825.
- Avila, A. M., Mezić, I., 2020. Data-driven analysis and forecasting of highway traffic dynamics. *Nature communications* 11 (1), 2090.
- Bae, B., Kim, H., Lim, H., Liu, Y., Han, L. D., Freeze, P. B., 2018. Missing data imputation for traffic flow speed using spatio-temporal cokriging. *Transportation Research Part C: Emerging Technologies* 88, 124–139.
- Bahadori, M. T., Yu, Q. R., Liu, Y., 2014. Fast multivariate spatio-temporal analysis via low rank tensor learning. *Advances in neural information processing systems* 27.
- Bellocchi, L., Geroliminis, N., 2020. Unraveling reaction-diffusion-like dynamics in urban congestion propagation: Insights from a large-scale road network. *Scientific reports* 10 (1), 4876.
- Benbarka, N., Höfer, T., Zell, A., et al., 2022. Seeing implicit neural representations as fourier series. In: *Proceedings of the IEEE/CVF Winter Conference on Applications of Computer Vision*. pp. 2041–2050.
- Chen, X., Chen, Y., Saunier, N., Sun, L., 2021a. Scalable low-rank tensor learning for spatiotemporal traffic data imputation. *Transportation Research Part C: Emerging Technologies* 129, 103226.
- Chen, X., Cheng, Z., Saunier, N., Sun, L., 2022. Laplacian convolutional representation for traffic time series imputation. *arXiv preprint arXiv:2212.01529*.
- Chen, X., He, Z., Chen, Y., Lu, Y., Wang, J., 2019a. Missing traffic data imputation and pattern discovery with a bayesian augmented tensor factorization model. *Transportation Research Part C: Emerging Technologies* 104, 66–77.
- Chen, X., He, Z., Sun, L., 2019b. A bayesian tensor decomposition approach for spatiotemporal traffic data imputation. *Transportation research part C: emerging technologies* 98, 73–84.
- Chen, X., Lei, M., Saunier, N., Sun, L., 2021b. Low-rank autoregressive tensor completion for spatiotemporal traffic data imputation. *IEEE Transactions on Intelligent Transportation Systems*, 1–10.
- Chen, X., Qin, G., Seo, T., Yin, J., Tian, Y., Sun, J., 2024. A macro-micro approach to reconstructing vehicle trajectories on multi-lane freeways with lane changing. *Transportation Research Part C: Emerging Technologies* 160, 104534.
- Chen, X., Yang, J., Sun, L., 2020. A nonconvex low-rank tensor completion model for spatiotemporal traffic data imputation. *Transportation Research Part C: Emerging Technologies* 117, 102673.
- Chen, Y., Liu, S., Wang, X., 2021c. Learning continuous image representation with local implicit image function. In: *Proceedings of the IEEE/CVF conference on computer vision and pattern recognition*. pp. 8628–8638.
- Cheng, Z., Trépanier, M., Sun, L., 2022. Real-time forecasting of metro origin-destination matrices with high-order weighted dynamic mode decomposition. *Transportation science* 56 (4), 904–918.
- Deng, L., Liu, X.-Y., Zheng, H., Feng, X., Chen, Y., 2021. Graph spectral regularized tensor completion for traffic data imputation. *IEEE Transactions on Intelligent Transportation Systems*, 1–15.
- Duan, J., Zeng, G., Serok, N., Li, D., Lieberthal, E. B., Huang, H.-J., Havlin, S., 2023. Spatiotemporal dynamics of traffic bottlenecks yields an early signal of heavy congestions. *Nature communications* 14 (1), 8002.
- Dupont, E., Goliński, A., Alizadeh, M., Teh, Y. W., Doucet, A., 2021. Coin: Compression with implicit neural representations. *arXiv preprint arXiv:2103.03123*.
- Fons, E., Sztrajman, A., El-Laham, Y., Iosifidis, A., Vyetenko, S., 2022. Hypertime: Implicit neural representation for time series. *arXiv preprint arXiv:2208.05836*.
- Fu, H., Lam, W. H., Ho, H., Ma, W., 2023. Optimization of multi-type traffic sensor locations for network-wide link travel time estimation with consideration of their covariance. *Transportmetrica B: Transport Dynamics* 11 (1), 760–782.
- Fu, H., Wang, Y., Tang, X., Zheng, N., Geroliminis, N., 2020. Empirical analysis of large-scale multimodal traffic with multi-sensor data. *Transportation Research Part C: Emerging Technologies* 118, 102725.
- Goulart, J. d. M., Kibangou, A., Favier, G., 2017. Traffic data imputation via tensor completion based on soft thresholding of tucker core. *Transportation Research Part C: Emerging Technologies* 85, 348–362.



- Grattarola, D., Vanderghenst, P., 2022. Generalised implicit neural representations. *Advances in Neural Information Processing Systems* 35, 30446–30458.
- Gunasekar, S., Woodworth, B. E., Bhojanapalli, S., Neyshabur, B., Srebro, N., 2017. Implicit regularization in matrix factorization. *Advances in neural information processing systems* 30.
- He, K., Zhang, X., Ren, S., Sun, J., 2016. Deep residual learning for image recognition. In: *Proceedings of the IEEE conference on computer vision and pattern recognition*. pp. 770–778.
- He, W., Zhang, H., Zhang, L., Shen, H., 2015. Total-variation-regularized low-rank matrix factorization for hyperspectral image restoration. *IEEE transactions on geoscience and remote sensing* 54 (1), 178–188.
- He, Z., Lv, Y., Lu, L., Guan, W., 2017. Constructing spatiotemporal speed contour diagrams: using rectangular or non-rectangular parallelogram cells? *Transportmetrica B: transport dynamics*.
- Hornik, K., 1991. Approximation capabilities of multilayer feedforward networks. *Neural networks* 4 (2), 251–257.
- Hu, Z., Ma, W., 2024. Demonstration-guided deep reinforcement learning for coordinated ramp metering and perimeter control in large scale networks. *Transportation research part C: emerging technologies* 159, 104461.
- Huang, A. J., Agarwal, S., 2020. Physics informed deep learning for traffic state estimation. In: *2020 IEEE 23rd International Conference on Intelligent Transportation Systems (ITSC)*. IEEE, pp. 1–6.
- Jacot, A., Gabriel, F., Hongler, C., 2018. Neural tangent kernel: Convergence and generalization in neural networks. *Advances in neural information processing systems* 31.
- Kolda, T. G., Bader, B. W., 2009. Tensor decompositions and applications. *SIAM review* 51 (3), 455–500.
- Lehmer, D., Dietrich, F., Köster, G., 2021. Modeling melburnians-using the koopman operator to gain insight into crowd dynamics. *Transportation Research Part C: Emerging Technologies* 133, 103437.
- Lei, M., Labbe, A., Wu, Y., Sun, L., 2022. Bayesian kernelized matrix factorization for spatiotemporal traffic data imputation and kriging. *IEEE Transactions on Intelligent Transportation Systems*, 1–13.
- Li, A., Lam, W. H., Ma, W., Chow, A. H., Wong, S.-C., Tam, M. L., 2023. Filtering limited automatic vehicle identification data for real-time path travel time estimation without ground truth. *IEEE Transactions on Intelligent Transportation Systems*.
- Liang, W., Li, Y., Xie, K., Zhang, D., Li, K.-C., Souri, A., Li, K., 2022a. Spatial-temporal aware inductive graph neural network for c-its data recovery. *IEEE Transactions on Intelligent Transportation Systems*.
- Liang, Y., Ouyang, K., Jing, L., Ruan, S., Liu, Y., Zhang, J., Rosenblum, D. S., Zheng, Y., 2019. Urbanfm: Inferring fine-grained urban flows. In: *Proceedings of the 25th ACM SIGKDD international conference on knowledge discovery & data mining*. pp. 3132–3142.
- Liang, Y., Zhao, Z., Sun, L., 2022b. Memory-augmented dynamic graph convolution networks for traffic data imputation with diverse missing patterns. *Transportation Research Part C: Emerging Technologies* 143, 103826.
- Liu, G., Zhang, W., 2022. Recovery of future data via convolution nuclear norm minimization. *IEEE Transactions on Information Theory* 69 (1), 650–665.
- Liu, J., Han, K., Chen, X. M., Ong, G. P., 2019. Spatial-temporal inference of urban traffic emissions based on taxi trajectories and multi-source urban data. *Transportation Research Part C: Emerging Technologies* 106, 145–165.
- Luo, X., Xu, W., Ren, Y., Yoo, S., Nadiga, B., 2024. Continuous field reconstruction from sparse observations with implicit neural networks. *arXiv preprint arXiv:2401.11611*.
- Luo, Y., Zhao, X., Li, Z., Ng, M. K., Meng, D., 2023. Low-rank tensor function representation for multi-dimensional data recovery. *IEEE Transactions on Pattern Analysis and Machine Intelligence*.
- Lyu, C., Lu, Q.-L., Wu, X., Antoniou, C., 2024. Tucker factorization-based tensor completion for robust traffic data imputation. *Transportation Research Part C: Emerging Technologies* 160, 104502.
- Mildenhall, B., Srinivasan, P. P., Tancik, M., Barron, J. T., Ramamoorthi, R., Ng, R., 2021. Nerf: Representing scenes as neural radiance fields for view synthesis. *Communications of the ACM* 65 (1), 99–106.
- Nallaperuma, D., Nawaratne, R., Bandaragoda, T., Adikari, A., Nguyen, S., Kempitiya, T., De Silva, D., Alahakoon, D., Pothuhera, D., 2019. Online incremental machine learning platform for big data-driven smart traffic management. *IEEE Transactions on Intelligent Transportation Systems* 20 (12), 4679–4690.
- Naour, E. L., Serrano, L., Migus, L., Yin, Y., Agoua, G., Baskiotis, N., Guigue, V., et al., 2023. Time series continuous modeling for imputation and forecasting with implicit neural representations. *arXiv preprint arXiv:2306.05880*.
- Nie, T., Qin, G., Mei, Y., Sun, J., 2023a. Imputeformer: Graph transformers for generalizable spatiotemporal imputation. *arXiv preprint arXiv:2312.01728*.
- Nie, T., Qin, G., Sun, J., 2022. Truncated tensor Schatten p-norm based approach for spatiotemporal traffic data imputation with complicated missing patterns. *Transportation Research Part C: Emerging Technologies* 141, 103737.
- Nie, T., Qin, G., Wang, Y., Sun, J., 2023b. Correlating sparse sensing for large-scale traffic speed estimation: A laplacian-enhanced low-rank tensor kriging approach. *Transportation Research Part C: Emerging Technologies* 152, 104190.
- Nie, T., Qin, G., Wang, Y., Sun, J., 2023c. Towards better traffic volume estimation: Jointly addressing the underdetermination and nonequilibrium problems with correlation-adaptive gnns. *Transportation Research Part C: Emerging Technologies* 157, 104402.

- Ortega, A., Frossard, P., Kovačević, J., Moura, J. M., Vandergheynst, P., 2018. Graph signal processing: Overview, challenges, and applications. *Proceedings of the IEEE* 106 (5), 808–828.
- Paipuri, M., Barmponakis, E., Geroliminis, N., Leclercq, L., 2021. Empirical observations of multi-modal network-level models: Insights from the pneuma experiment. *Transportation Research Part C: Emerging Technologies* 131, 103300.
- Qin, G., Huang, Z., Xiang, Y., Sun, J., 2019. Probdetect: A choice probability-based taxi trip anomaly detection model considering traffic variability. *Transportation Research Part C: Emerging Technologies* 98, 221–238.
- Rahaman, N., Baratin, A., Arpit, D., Draxler, F., Lin, M., Hamprecht, F., Bengio, Y., Courville, A., 2019. On the spectral bias of neural networks. In: *International conference on machine learning*. PMLR, pp. 5301–5310.
- Raissi, M., Perdikaris, P., Karniadakis, G. E., 2019. Physics-informed neural networks: A deep learning framework for solving forward and inverse problems involving nonlinear partial differential equations. *Journal of Computational Physics* 378, 686–707.
- Rao, N., Yu, H.-F., Ravikumar, P. K., Dhillon, I. S., 2015. Collaborative filtering with graph information: Consistency and scalable methods. *Advances in neural information processing systems* 28.
- Rossi, E., Kenlay, H., Gorinova, M. I., Chamberlain, B. P., Dong, X., Bronstein, M. M., 2022. On the unreasonable effectiveness of feature propagation in learning on graphs with missing node features. In: *Learning on Graphs Conference*. PMLR, pp. 11–1.
- Roy, O., Vetterli, M., 2007. The effective rank: A measure of effective dimensionality. In: *2007 15th European signal processing conference*. IEEE, pp. 606–610.
- Saberi, M., Hamedmoghadam, H., Ashfaq, M., Hosseini, S. A., Gu, Z., Shafiei, S., Nair, D. J., Dixit, V., Gardner, L., Waller, S. T., et al., 2020. A simple contagion process describes spreading of traffic jams in urban networks. *Nature communications* 11 (1), 1616.
- Saeedmanesh, M., Kouvelas, A., Geroliminis, N., 2021. An extended kalman filter approach for real-time state estimation in multi-region mfd urban networks. *Transportation Research Part C: Emerging Technologies* 132, 103384.
- Sen, R., Yu, H.-F., Dhillon, I. S., 2019. Think globally, act locally: A deep neural network approach to high-dimensional time series forecasting. *Advances in neural information processing systems* 32.
- Shi, R., Mo, Z., Di, X., 2021. Physics-informed deep learning for traffic state estimation: A hybrid paradigm informed by second-order traffic models. In: *Proceedings of the AAAI Conference on Artificial Intelligence*. Vol. 35. pp. 540–547.
- Sitzmann, V., Martel, J., Bergman, A., Lindell, D., Wetzstein, G., 2020. Implicit neural representations with periodic activation functions. *Advances in neural information processing systems* 33, 7462–7473.
- Sofuoglu, S. E., Aviyente, S., 2022. Gloss: Tensor-based anomaly detection in spatiotemporal urban traffic data. *Signal Processing* 192, 108370.
- Tan, H., Feng, G., Feng, J., Wang, W., Zhang, Y.-J., Li, F., 2013. A tensor-based method for missing traffic data completion. *Transportation Research Part C: Emerging Technologies* 28, 15–27.
- Tancik, M., Srinivasan, P., Mildenhall, B., Fridovich-Keil, S., Raghavan, N., Singhal, U., Ramamoorthi, R., Barron, J., Ng, R., 2020. Fourier features let networks learn high frequency functions in low dimensional domains. *Advances in neural information processing systems* 33, 7537–7547.
- Thibeault, V., Allard, A., Desrosiers, P., 2024. The low-rank hypothesis of complex systems. *Nature Physics*, 1–9.
- Thodi, B. T., Ambadipudi, S. V. R., Jabari, S. E., 2024. Fourier neural operator for learning solutions to macroscopic traffic flow models: Application to the forward and inverse problems. *Transportation Research Part C: Emerging Technologies* 160, 104500.
- Treiber, M., Kesting, A., 2013. *Traffic flow dynamics. Traffic Flow Dynamics: Data, Models and Simulation*, Springer-Verlag Berlin Heidelberg, 983–1000.
- Tsitsokas, D., Kouvelas, A., Geroliminis, N., 2023. Two-layer adaptive signal control framework for large-scale dynamically-congested networks: Combining efficient max pressure with perimeter control. *Transportation Research Part C: Emerging Technologies* 152, 104128.
- Wang, X., Jerome, Z., Wang, Z., Zhang, C., Shen, S., Kumar, V. V., Bai, F., Krajewski, P., Deneau, D., Jawad, A., et al., 2024. Traffic light optimization with low penetration rate vehicle trajectory data. *Nature communications* 15 (1), 1306.
- Wang, X., Miranda-Moreno, L., Sun, L., 2021. Hankel-structured tensor robust pca for multivariate traffic time series anomaly detection. *arXiv preprint arXiv:2110.04352*.
- Wang, X., Sun, L., 2023. Anti-circulant dynamic mode decomposition with sparsity-promoting for highway traffic dynamics analysis. *Transportation research part C: emerging technologies* 153, 104178.
- Wang, X., Wu, Y., Zhuang, D., Sun, L., 2023. Low-rank hankel tensor completion for traffic speed estimation. *IEEE Transactions on Intelligent Transportation Systems* 24 (5), 4862–4871.
- Wang, Y., Zhang, Y., Piao, X., Liu, H., Zhang, K., 2018. Traffic data reconstruction via adaptive spatial-temporal correlations. *IEEE Transactions on Intelligent Transportation Systems* 20 (4), 1531–1543.
- Woo, G., Liu, C., Sahoo, D., Kumar, A., Hoi, S., 2023. Learning deep time-index models for time series forecasting. In: *International Conference on Machine Learning*. PMLR, pp. 37217–37237.
- Wu, T., Gao, X., An, F., Sun, X., An, H., Su, Z., Gupta, S., Gao, J., Kurths, J., 2024. Predicting multiple observations in complex systems through low-dimensional embeddings. *Nature Communications* 15 (1), 2242.
- Wu, Y., Zhuang, D., Labbe, A., Sun, L., 2021. Inductive graph neural networks for spatiotemporal kriging. In: *Proceedings of the AAAI Conference on Artificial Intelligence*. Vol. 35. pp. 4478–4485.

- Xing, J., Liu, R., Anish, K., Liu, Z., 2023. A customized data fusion tensor approach for interval-wise missing network volume imputation. *IEEE Transactions on Intelligent Transportation Systems*.
- Xu, Z.-Q. J., Zhang, Y., Luo, T., Xiao, Y., Ma, Z., 2019. Frequency principle: Fourier analysis sheds light on deep neural networks. arXiv preprint arXiv:1901.06523.
- Yang, J.-M., Peng, Z.-R., Lin, L., 2021. Real-time spatiotemporal prediction and imputation of traffic status based on lstm and graph laplacian regularized matrix factorization. *Transportation Research Part C: Emerging Technologies* 129, 103228.
- Ye, Q., Szeto, W. Y., Wong, S. C., 2012. Short-term traffic speed forecasting based on data recorded at irregular intervals. *IEEE Transactions on Intelligent Transportation Systems* 13 (4), 1727–1737.
- Yu, H.-F., Rao, N., Dhillon, I. S., 2016. Temporal regularized matrix factorization for high-dimensional time series prediction. *Advances in neural information processing systems* 29.
- Yu, J., Stettler, M. E., Angeloudis, P., Hu, S., Chen, X. M., 2020. Urban network-wide traffic speed estimation with massive ride-sourcing gps traces. *Transportation Research Part C: Emerging Technologies* 112, 136–152.
- Yuan, H., Li, G., 2021. A survey of traffic prediction: from spatio-temporal data to intelligent transportation. *Data Science and Engineering* 6 (1), 63–85.
- Zhang, H., Chen, P., Zheng, J., Zhu, J., Yu, G., Wang, Y., Liu, H. X., 2019. Missing data detection and imputation for urban anpr system using an iterative tensor decomposition approach. *Transportation Research Part C: Emerging Technologies* 107, 337–355.
- Zhang, J., Che, H., Chen, F., Ma, W., He, Z., 2021. Short-term origin-destination demand prediction in urban rail transit systems: A channel-wise attentive split-convolutional neural network method. *Transportation Research Part C: Emerging Technologies* 124, 102928.
- Zhang, J., Mao, S., Yang, L., Ma, W., Li, S., Gao, Z., 2024. Physics-informed deep learning for traffic state estimation based on the traffic flow model and computational graph method. *Information Fusion* 101, 101971.
- Zhang, J., Wang, F.-Y., Wang, K., Lin, W.-H., Xu, X., Chen, C., 2011. Data-driven intelligent transportation systems: A survey. *IEEE Transactions on Intelligent Transportation Systems* 12 (4), 1624–1639.
- Zhang, Y., Cheng, Q., Liu, Y., Liu, Z., 2022. Full-scale spatio-temporal traffic flow estimation for city-wide networks: a transfer learning based approach. *Transportmetrica B: Transport Dynamics*, 1–27.
- Zhang, Z., Li, M., Lin, X., Wang, Y., 2020. Network-wide traffic flow estimation with insufficient volume detection and crowdsourcing data. *Transportation Research Part C: Emerging Technologies* 121, 102870.
- Zheng, Z., Wang, Z., Hu, Z., Wan, Z., Ma, W., 2024. Recovering traffic data from the corrupted noise: A doubly physics-regularized denoising diffusion model. *Transportation Research Part C: Emerging Technologies* 160, 104513.